Aircraft electric propulsion systems: Alternative energy storage and electric motors

Rodrigo Muchagato Figueiredo

Thesis to obtain the Master of Science Degree in

Electrical and Computer Engineering

Supervisor: Prof. João Filipe Pereira Fernandes

Examination Committee

Chairperson: Profª. Célia Maria Santos Cardoso de Jesus
Supervisor: Prof. João Filipe Pereira Fernandes
Member of the Committee: Prof. Paulo José da Costa Branco

November 2022

Declarations

I declare that this document is an original work of my own authorship and that it fulfills all the requirements of the Code of Conduct and Good Practices of the Universidade de Lisboa.

Acknowledgments

This thesis marks the end of a significant chapter in my life. This 5-year journey was not easy but it feels right to finish it and remember all the challenges I have been through. I have grown a lot and learned so much, but most importantly, I met significant people that without them, it would have been very different.

To Catarina, I can't thank you enough for always being there for me. Your strength, passion and encouragement made this journey way easier. Without your constant moral and emotional support, I would not be who I am today neither be where I am today. You inspire me every day to overcome myself and give me the strength to become a better person.

To my family, I want to thank my mother and my father for helping me follow my dream with your support and hard-working example. To my brother, for pulling out of me my hardworking side to give you the best example I can. A very special thanks to my grandmother and my grandfather for being my second parents and a wonderful example - I owe you who I am today.

To my supervisor, Prof. João Fernandes, I cannot express how grateful I am for having you guiding me during the past year. Your availability, dedication and passion for what you do every day are an additional strength and an inspiration for those who work with you. To Prof. Paulo Branco, I wish you could have followed the entire thesis work, but the initial assistance provided was greatly appreciated.

To my friends from Técnico, that thrilled this path together with me. Thanks for all the help and cheeriness either during long academic evaluations or in life in general. It would not be possible to achieve this without your help.

To the closest friends that I made in Delft, you also had an impact on this work. Thanks for the support, the friendship but mainly for making me feel at home in a different country.

Abstract

Current aircraft are responsible for a high share of the total CO_2 emissions and noise pollution. With the continuous growth of the aeronautical sector, it is mandatory to take some actions to mitigate climate change. Therefore, the European Commission has set goals for reducing gas emissions in the aeronautical sector to be achieved by 2050. NASA also proposed a strategic implementation plan but to be achieved by 2035. For this, improvements and innovations on the current aircraft are urgent. One possible way to achieve these objectives is the electrification of the aircraft sector.

With the work developed in this thesis, it is intended to elaborate a comparative study between several energy storage systems and electric motors to be installed on existing aircraft. These models are to be complemented with different aircraft aerodynamic models to allow the estimation of the required energy and power in a flight simulation. The scenarios of take-off and cruising are addressed in this work for three different aircraft models.

Results show that electrification for Unmanned Aerial Vehicles and small aircraft is today possible, but with a limited range. For commercial aircraft, the superconducting motors combined with fuel cells show some potential, however, these technologies are still under development.

Keywords

Electric Aircraft; Electric Motors; Energy Storage Systems; Modelation; Simulation.

Resumo

Atualmente, o setor da aviação é responsável por uma grande parte das emissões de CO_2 e de ruído. Com o contínuo crescimento do setor, é urgente a implementação de algumas medidas para mitigar as alterações climáticas. Deste modo, a Comissão Europeia definiu objetivos a atingir em 2050 que visam a redução da emissão de gases poluentes no setor aeronáutico. A NASA também propôs um plano de implementação estratégica, mas com o objetivo de ser atingido em 2035. Para tal, é crucial o desenvolvimento e a inovação nos aviões atuais. Um caminho possível para atingir estes objetivos tem por base a eletrificação de aviões.

Com o trabalho desenvolvido nesta tese, pretende-se elaborar um estudo comparativo entre alguns tipos de sistemas de armazenamento de energia e de motores elétricos a serem instalados em aviões elétricos. Estes modelos serão complementados com diversos modelos aerodinâmicos de aviões de modo a estimar o consumo de energia e potência com a simulação de uma trajetória de voo realista. Os cenários de descolagem e cruzeiro são abordados nesta implementação para três modelos de aviões.

Os resultados obtidos mostram que a eletrificação para Unmanned Aerial Vehicles e aviões de pequeno porte é possível hoje em dia, porém com um alcance limitado. Para aviões comerciais, a utilização de motores supercondutores com fuel cells demonstra algum potencial, porém estas tecnologias ainda estão sob desenvolvimento.

Palavras Chave

Aviões Elétricos; Modelação; Motores Elétricos; Simulação; Sistemas de Armazenamento de Energia

Contents

List of Figures

List of Tables

Acronyms

AC Alternating Current

AEA All-electric Aircraft

APU Auxiliary Power Unit

BLDC Brushless DC

CE Coulombic Efficiency

DC Direct Current

EV Electric Vehicle

ESS Energy Storage System

ECS Environmental Control Systems

EFTA European Free Trade Association

EU European Union

FOC Field Oriented Control

HEA Hybrid-electric Aircraft

HEV Hybrid-electric Vehicle

HTS High Temperature Superconductors

IM Induction Motor

MEA More-electric Aircraft

PMSM Permanent Magnet Synchronous Motor

PID Proportional, Integral and Derivative

RC Radio-controlled

RBCC Reverse-Brayton Cycle Cryocooler

SOC State of Charge

SM	Synchronous Machine
UAV	Unmanned Aerial Vehicle

Nomenclature

Greek symbols

α Angle of Attack.

β Heading Angle.

η Efficiency.

γ Flight Path Angle.

λ Magnetic Flux.

μ Bank Angle.

ω Rotational Speed in rad/s.

ρ_{air} Air density.

θ Pitch Angle.

Roman symbols

$\vec{A}$ Aerodynamic Forces.

$\vec{a}$ Acceleration.

C_D Drag Coefficient.

C_L Lift Coefficient.

C_T Thrust Coefficient.

$\vec{D}$ Drag.

D_p Propeller Diameter.

E Energy.

$\overrightarrow{F_r}$ Resultant Force.

$\overrightarrow{F_T}$ Thrust Force.

g Acceleration of gravity.

I Current.

i, j, k Unitary Vectors of the Orthogonal Coordinate System.

J Advance Ratio.

$\vec{L}$ Lift.

L Inductance.

M Mass.

$\vec{N}$ Normal Reaction Force.

n Rotational Speed in rpm.

n_{pp} Number of pole pairs.

P Power.

q Dynamic Pressure.

R Resistance.

S Wing Surface Area.

T Torque.

t Time.

U, v Voltage.

$\vec{V}$ Linear Velocity.

$\vec{W}$ Weight.

x, y, z Position of the aircraft.

Subscripts

0 Initial condition.

$aero$ Regarding Aerodynamic System.

b Regarding Battery System.

b Relative to the body axis system.

Cu Relative to the copper material.

d, q Relative to direct and quadrature axis.

$e.e.$ Regarding Electronic Equipment.

Fe Relative to the iron material.

h Relative to the local horizon axis system.

m Regarding Motor System.

N Relative to nominal conditions.

p Regarding Propeller System.

PM Relative to permanent magnets.

w Relative to the wind axis system.

x Relative to the x axis.

y Relative to the y axis.

z Relative to the z axis.

Superscripts

0 Under no-load conditions.

1

Introduction

Contents

1.1 Motivation

The number of flights in the European Union (EU) and European Free Trade Association (EFTA) has increased by 8% between 2014 and 2017 and, in the most-likely forecast, it is expected a growth of 42% until 2040 [1]. As a consequence of this growth, it is foreseen that by 2050 the fuel consumption will have increased by a factor between 2.4 and 3.8 [2] resulting in an increase of CO_2 and NO_X emissions of at least 21% and 16% respectively [1], compared with 2019.

Aviation constitutes about 2.5% of all energy-related CO_2 emissions [3] and during 2015, international flights consumed around 160 Mton of fuel, resulting in the emission of 506 Mton of CO_2 [2]. Looking at the whole transportation sector, aviation is responsible for around 13.4% of the total sector's emissions [1].

Noise is also an important source of pollution. It is estimated that, in 2017, around 3.2 million people were highly affected by aircraft noise and 1.4 million suffered from high sleep disturbance around the 47 major airports [1]. According to the World Health Organization, sound levels below 70 dB do not damage living organisms, regardless of how long or consistent the exposure is [4]. However, the number of people exposed to more than 50 aircraft noise events exceeding 70 dB per day was estimated to be 1 million in 2017 for the same airports and this is 60% more than in 2005 [1].

For all these reasons, it is urgent to implement changes in the sector because passenger numbers are growing faster and faster. In 2017, for example, there were 50% more passengers and 14% more scheduled flights than in 2005 [1]. Therefore, as an incentive to attenuate the impacts of the aviation sector, goals have been set by the European Commission to be achieved by 2050. These objectives include a reduction of 75% in CO_2 emissions, 90% in NO_x and 65% in noise emission [5]. On top of that, in 2019, NASA has also set equivalent objectives but for 2035 [6]. These goals and strategies aim not only for improvements to the existing aircraft but also to encourage research and development of new types of aircraft like All-electric Aircraft (AEA), Hybrid-electric Aircraft (HEA) and More-electric Aircraft (MEA).

1.2 Goals

Following the goals proposed by the European Commission and NASA, this work will focus on the efficiency and feasibility assessment of AEA, using different sources of energy. To accomplish this, the following goals are set:

- Development of a simulation tool for an electric aircraft and respective testing for flight performance.

- Testing the flight performance regarding energy consumption using different energy storage systems - $LiFePO_4$ batteries and fuel cells.
- Testing the influence of using alternative electric motors for the fans propulsion - Permanent Magnet Synchronous Motor (PMSM) and superconducting motors.

1.3 Thesis Outline

This thesis is structured as follows:

- **Chapter 1 - Introduction** - This chapter includes the motivation and the goals to be achieved in this thesis.
- **Chapter 2 - Background and State of the Art** - Here, an overview on the background and state of the art of the topics required for this thesis are presented. Starting on the types of electrical aircraft, three types are going to be studied - MEA, HEA and AEA. Then, regarding Energy Storage System (ESS), the topics introduced are batteries and fuel cells. Moreover, the study on electric motors will include a comparison between Induction Motor (IM) and PMSM, the hypothesis of using Cryogenic and Superconducting motors as well as the types of models used to describe electric motors. Lastly, the type of propellers for electric motors will be addressed.
- **Chapter 3 - Model of the Systems** - In this chapter, the implementation of the different system's models is going to be detailed. There are going to be developed four consecutive systems: Aerodynamic, Propeller, Electric Motor and ESS.
- **Chapter 4 - Results** - After the implementation of the systems, the results are shown. Three different aircraft will be modelled and the respective results presented.
- **Chapter 5 - Conclusion and Future Work** - Last, but not least, this thesis is concluded and highlights the future work to be performed.

2

Background and State of the Art

Contents

2.1 Types of Electrical Aircraft

In this section, different types of electric aircraft will be described as well as the conventional aircraft that are used nowadays. The electric aircraft include the More-electric Aircraft (MEA), the Hybrid-electric Aircraft (HEA) and the All-electric Aircraft (AEA).

2.1.1 Conventional aircrafts

Conventional aircraft that are used nowadays use a combination of mechanical, hydraulic, pneumatic and electrical systems, where the main energy source to feed them is fuel [7]. The energy stored in the fuel is converted to propulsive power and heat dissipation in the engines and is also used to supply loads of the auxiliary systems. These auxiliary systems perform crucial roles such as supplying hot air for anti-icing systems and flight control mechanisms, deploying the landing gear, aircraft lighting and Environmental Control Systems (ECS) [8].

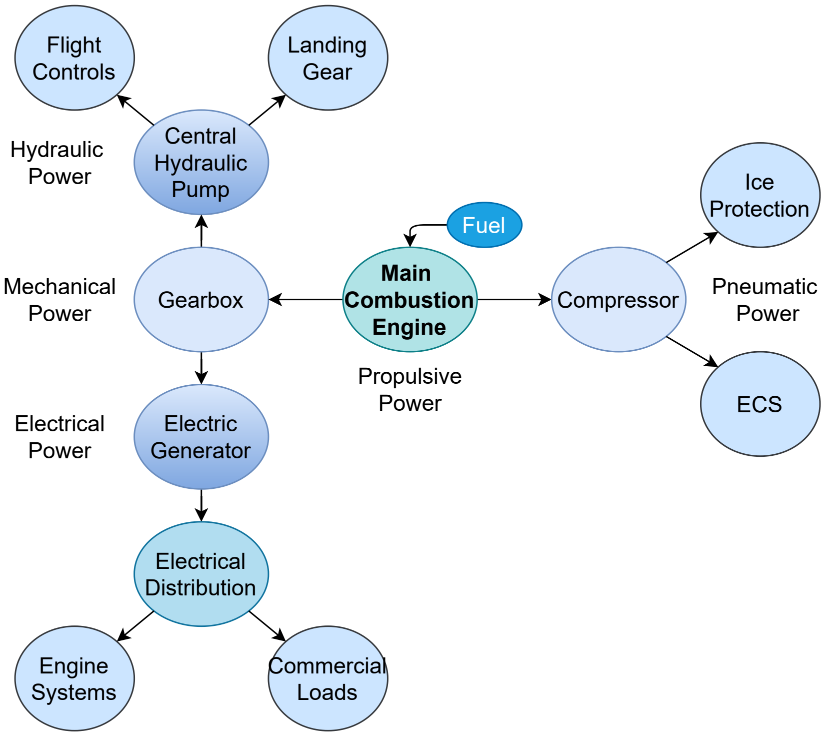

Figure 2.1: Schematic of an aircraft's conventional power distribution. Adapted from [7].

All these systems are very complex, and thus hard to implement and interconnect. Also, the large number of sub-systems tends to decrease the overall efficiency and increase the chances of occurring failures [7]. Therefore, there is an effort from the aircraft companies and the EU to move to AEA where all the power used in the aircraft is generated from electrical sources.

The Boeing 737 (Figure 2.2) is on the top-5 of most produced commercial aircraft in history with more than 10 000 units [9]. This aircraft uses two turbofan engines, can transport up to 220 passengers on the version 737-900ER [10] and has a flight range of around 5450 kilometers with 178 passenger seats that can be used [11].

Figure 2.2: Boeing 737 [10].

Just during 2019, this aircraft model was responsible for total emissions of 16.3 Mton of CO_2 for all passengers transported [12]. Since a typical passenger vehicle emits about 4.6 metric tons of carbon dioxide per year [13], the emissions for this type of aircraft are equivalent to the emissions of 3540 typical passenger vehicles.

However, there are still some technological barriers to the implementation of AEA. Thus, intermediate solutions such as MEA and HEA are currently being implemented in the market.

2.1.2 More-electric Aircraft

For the past years, there has been a considerable change in the system design of aircraft. Electrical systems are increasingly being used in many applications like aircraft actuation systems, wing ice protection systems and fuel pumping. In the past, these and many other mechanisms were powered by hydraulic, mechanical, or pneumatic power sources. This is opening doors to a world where aircraft are quieter, lighter and more fuel-efficient, improving the environment for everyone as well as reducing maintenance costs [14].

In Figure 2.3, a schematic of a MEA power distribution can be seen. Here the electrical power is feeding many systems, whereas in Figure 2.1 hydraulic and pneumatic power was also used as a source.

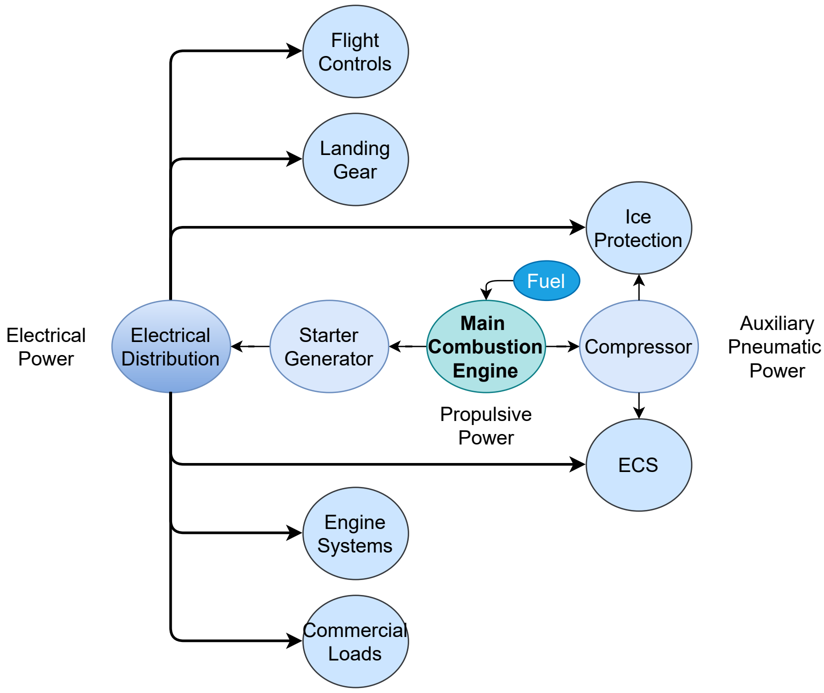

Figure 2.3: Schematic of a More-electric Aircraft power distribution. Adapted from [7].

ECS and ice protection are crucial systems, therefore there is a redundancy, with both electric and pneumatic power, for a case of electric failure. In these types of aircraft, there is also one Auxiliary Power Unit (APU) with a gas turbine in the aircraft's tail used to start up the motors.

For example, the fly-by-wire flight control system is an electric flight control system that is replacing its equivalent conventional system. It employees feedback such that the vehicle motion is the controlled parameter. The movements of flight controls are converter to electronic signals and transmitted by wires through the aircraft. Flight control computers are in charge of determining how to move the aircraft actuators at each control surface to provide the demanded response. A supplementary mechanical backup system can also be used in pseudo-fly-by-wire systems [15].

Two successful examples of this implementation are the Boeing 787 [16] and the Airbus A380 [17] where variable frequency starter-generators are mechanically coupled to the aircraft's fuel engines to supply these auxiliary systems.

2.1.3 Hybrid-electric Aircraft

A HEA is an aircraft where electrical and mechanical are both energy sources. Since the energy density of lithium-ion batteries is much lower than fuel and the hydrogen fuel cell technology has still some barriers to its massive implementation on aircraft, the combination of both engine types may be a good equilibrium between conventional aircraft and AEA.

There are several degrees of hybridization that can be classified according to electric motor power and energy source usage. On one side of the spectrum, there are all-electric aircraft - which only use electrical energy and power for propulsion - and, on the opposite side, there are the conventional aircraft that use no electric power or electric energy for propulsion. HEA relies on a mix of fuel and electrical energy storage and propulsive power [18].

There can be series and parallel configurations inside these types of HEA. In the series connection (Figure 2.4), there are only electric motors that are mechanically connected to the propellers. The internal combustion engine, which runs with fuel, drives an electrical generator, which electrical output either drives the electric motor or charges the electric energy source. The main advantage of this architecture is that the combustion engine is not mechanically coupled to the propeller, therefore it can run constantly at its best operation power and speed [19].

Another topology is the parallel connection shown in Figure 2.5 where there are two parallel propulsion shafts connected through a mechanical coupling. There is one electric motor powered by the electric energy storage system and one fuel-powered combustion engine and they can both drive the propeller. In this case, it is also possible to charge the batteries when the combustion engine drives the propeller and the electric motor at the same time [19].

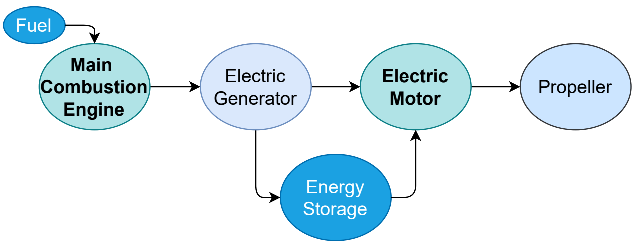

Figure 2.4: Scheme of the series-Hybrid-electric Aircraft configuration. Adapted from [19].

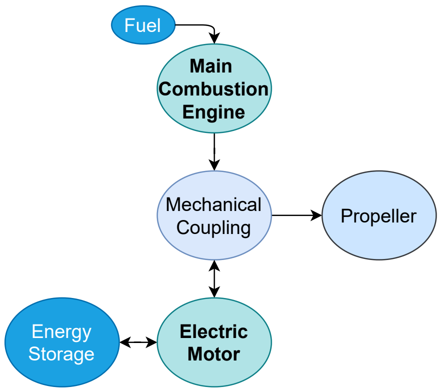

Figure 2.5: Scheme of the parallel-Hybrid-electric Aircraft configuration. Adapted from [19].

In general, series-connected HEA will perform worst than the parallel-connected for a similar set of parameters. This is caused by the additional mass of the generator as well as a reduction in the propulsive efficiency [20]. Batteries (or any other storage system) usually play an important role in these models to increase the reliability of the systems' supply.

As an example, STARC-ABL, represented in Figure 2.6, is passenger commercial concept aircraft developed by NASA. Its structure is very similar to the conventional aircraft with two engines mounted under each wing and the main body where the passengers sit. This model relies on turbo-electric propulsion, meaning that it uses electric motors powered by onboard gas turbines. It uses two traditional jet engines under the wings that also contain an electric generator. The generated electric power is sent to the tail of the aircraft which is an all-electric propulsor. This configuration reduces drag and improves fuel efficiency [21]. This parallel-hybrid model is still under development and is expected to be available between 2030 to 2035 with a cruising speed of 0.7 Mach (835 km/h) and a range of 6482 km [22].

Figure 2.6: STARC-ABL Concept [21].

Another concept developed by NASA, the N3-X (Figure 2.7) makes use of the so-called ”hybrid wing body” where the wing blends seamlessly into the body of the aircraft, which makes it extremely aerodynamic and holds great promise for dramatic reductions in fuel consumption, noise and emissions [23]. This turbo-electric aircraft has a cruising speed of 0.84 Mach (1037 km/h), an expected range of 13890 km and carries 300 passengers [22]. The technology proposed for the propulsion is a superconducting one, using 16 motors distributed through the aircraft's tail, all supplied by turboshaft engines, each in the tip of the wing. There are two electrical generators, also superconducting that are coupled with the turboshaft engines [24].

Figure 2.7: NASA N3-X Concept [23].

2.1.4 All-electric Aircraft

The AEA uses only an electric energy source for propulsion. This can be either by energy stored in batteries or by using fuel cells with liquid hydrogen. In Figure 2.8, it can be seen a scheme of the power configuration of AEA.

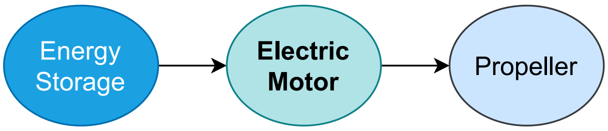

Figure 2.8: All-electric aircraft configuration. Adapted from [19].

Using batteries in either HEA or AEA can be challenging as they require around 32 times more weight and 10 times more volume to supply the same energy source of kerosene [25]. Therefore, fuel cells can be a good candidate for AEA applications due to their higher mass-specific energy as will be seen in Section 2.2.

Regarding propulsion systems, it is required at least 10 kW/kg of specific power for passenger-class aircraft. For context, Electric Vehicle (EV)'s motors have specific power of around 2 kW/kg and nowadays aircraft around 5 kW/kg [26].

On June 10th 2020, the Pipistrel's Velis Electro (Figure 2.9) became the first fully electric aircraft to receive its certification. This is a two-seat aircraft with a cruise speed of 90 knots (166 km/h) and endurance of up to 50 minutes [27]. A 57.6 kW liquid-cooled electric engine provides power to the aircraft and the power is delivered by a 345 V_{DC} electric system built around a liquid-cooled in-house developed high-performance battery system with a total nominal capacity of 24.8 kWh [28].

Figure 2.9: Pipistrel's Velis Electro [28].

2.2 Energy Storage Systems

An ESS is an apparatus that stores energy so that it can be used later on when needed. It can be stored as chemical, potential, electrical potential, heat or kinetic, for example. All these systems are defined by the density of energy and power that they are capable of storing [29].

In the following sub-sections, two systems will be studied - batteries and fuel cells.

2.2.1 Batteries

A battery is a device that stores chemical energy and converts it into electric energy by an electrochemical oxidation-reduction (redox) reaction. This type of reaction involves the transfer of electrons from the cathode (positive terminal) to the anode (negative terminal) via an electric circuit that is where the electric energy is to be used [30].

They are made of many cells connected in series or parallel, depending on the application. Series connection is used to increase the voltage by connecting the anode of one cell to the cathode of the other. On the other side, a parallel connection is implemented for higher current and capacity applications. Note that for this topology, all the cells have to have the same nominal voltage and the same charge level [30]. In most of the applications, a combination of series and parallel are used in order to increase the voltage, current and capacity at the same time.

There are two main figures of merit for batteries - the Coulombic Efficiency (CE) and Voltage Efficiency. The first (also called Faradaic Efficiency) is the ratio of the total charge extracted from the battery to the total charge put into the battery over a full cycle. Voltage Efficiency represents the ratio between the average discharge voltage and the average charge voltage [31].

Several types of batteries can be identified but the ones that are mostly used are zinc-carbon (Zn-C), alkaline, nickel-cadmium (NiCd), nickel-metal hydride (NiMH) and lithium-ion (Li-ion). Some of them, such as NiCd contain toxic metals so they should be properly discarded [32]. Also, the cathode of lithium-ion batteries contains a toxic and flammable electrolyte made of lithium salts ($LiClO_4$ and $LiPF_6$), organic chemicals and plastics [33]. Although, studies are being made to recycle Li-ion batteries [34].

In Figure 2.10 several types of Energy Storage systems can be seen with their respective energy and power densities. For this thesis, only batteries and fuel cells will be studied.

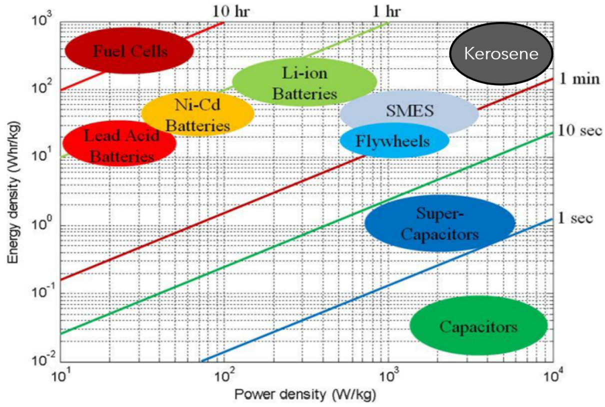

Figure 2.10: Energy density and Power density for different Energy Storage Systems. Adapted from [35].

Inside the batteries, the two best models are the Li-ion and the Ni-Cd because they can accomplish a high power and energy density. However, their prices are very high and, depending on the application, the investment may not be worth it. On the other side, the Lead-Acid batteries are the cheapest but they require, at least, monthly maintenance and check-up. Hence, they are mainly used in cases where cost-effectiveness, reliability, and abuse tolerance are critical but energy density and lifetime are not as important [36]. They also perform with a low CE, around 90% [31], and have a very low energy density. For aeronautical applications, weight is a critical factor, therefore, this type of battery is not feasible as it would require much more weight than others.

The NiMH type of battery is made of a nickel-oxyhydroxide–based positive electrode metallic cadmium–based negative electrode, and an alkaline electrolyte. It is used in some EVs and Hybrid-electric Vehicles (HEVs), however, a drawback is that it does not support fast charges or discharges [36]. Furthermore, their CE is the lowest, around 80% [37].

The Li-Ion batteries store charge (charging) by inserting Li-ions into a negative electrode and they supply power (discharging) by when the Li-ions move to the positive electrode. Well-known for their high energy and power density, high efficiency and long cycle life, they are also environmental friendly. Such attractive attributes, make them widely used in portable electronics and the most recent EVs and plug-in HEVs [36]. The most promising model is the $LiMn_2O_4$ that can achieve up to 200 Wh/kg of energy density [38]. This type offers the highest CE rating in rechargeable batteries, reaching up to 99%. However, this is only possible when charged at moderate currents and cold temperatures [31]. An important drawback is that Lithium is a rare material, therefore, it has to be used consciously.

2.2.2 Fuel cells

A fuel cell converts chemical energy stored in a fuel into electrical energy with hydrogen combustion that is split into two electrochemical reactions:

$$\mathrm{H_2} \rightleftharpoons 2\,\mathrm{H^+} + 2\,\mathrm{e^-} \tag{2.1}$$

$$\frac{1}{2}\,\mathrm{O_2} + 2\,\mathrm{H^+} + 2\,\mathrm{e^-} \rightleftharpoons \mathrm{H_2O} \tag{2.2}$$

By separating spatially these two reactions, it is possible to generate a current of electrons that will flow through an external circuit - the load. This spatial separation is done by making use of an electrolyte [39].

In Figure 2.11, a simple $H_2 - O_2$ fuel cell can be seen. In this case, there are two metallic electrodes dipped inside sulfuric acid, that works as the electrolyte. Molecules of hydrogen gas are injected into the left electrode and are going to be split into protons and electrons. Electrons will not be able to flow through the electrolyte but protons can. Therefore electrons will run through the external circuit and protons will recombine with electrons from the external circuit on the right electrode with oxygen gas that is pumped, accomplishing Equation (2.2).

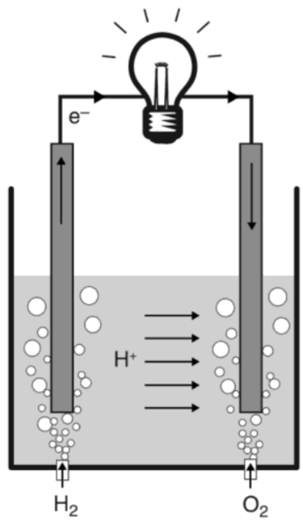

Figure 2.11: Fuel cell process illustration [39].

Fuel cells come up with a clean and efficient mechanism for energy conversion. Furthermore, they are compatible with renewable energy sources and energy carriers (hydrogen, for example) [40].

Different types of fuel cells have to be carefully chosen according to their operating temperature, efficiency, applications and costs. The alkaline fuel cell type is the most efficient (60%), followed by the polymer electrolyte membrane (58%) and Molten carbonate (47%). In terms of cost, Direct Methanol fuel cells and Phosphoric acid fuel cells are the cheapest, however, they do not achieve high efficiencies [41]. Studies are being done that show improvement in the efficiency to around 71% [42, 43]

2.2.3 Comparison of performance between batteries and fuel cells

When choosing an energy storage system, the most important parameters that should be analysed are the power density, the energy density, temperature limits for their operation, the number of charging and discharging cycles, its tolerance to overload and the cost that that technology will have for the project. Hence, in Table 2.1 different battery types and fuel cell above discussed are compared. This table will be useful, further on during this thesis, to choose the best technology for a possible implementation. In the lifetime, the criteria is different between batteries and fuel cells. For batteries, the number of cycles is shown for an 80% discharge whilst for fuel cells it is the number of operating hours in order to lose 10% of the power.

Characteristic	Lead-Acid batteries	Ni-Cd batteries	Li-ion batteries	Fuel cells
Energy Density [Wh/kg]	7 - 30	11 - 100	40 - 250	200 - 800
Power Density [W/kg]	10 - 50	30 - 105	100 - 180	10 - 70
Temperature Limits [°C]	-20 - 50	-20 - 65	-20 - 60	60 - 1000
Lifetime	200 - 300 cycles	1000 cycles	500 - 2000 cycles	1500 - 10000 hours
Tolerance to overload	High	Moderate	Very low	High
Price	300 - 600 $/kWh	1000 $/kWh	900 - 1300 $/kWh	1500 - 3000 $/kW

Table 2.1: Comparison between different batteries and fuel cells. Adapted from [35, 41, 44–47]

2.3 Electric Motors

An electric motor is an electric machine that is able to convert electrical energy to mechanical energy through a rotating shaft. There are many types of electric motors, and, in this section, there are going to be listed the main advantages and disadvantages of each of them for an aeronautical application.

2.3.1 Brushless DC Motor

The Brushless DC (BLDC) motor is also known as a synchronous DC motor, meaning that it uses a Direct Current (DC) electric power supply. This type of motor does not use brushes because the coils are not located on the rotor, so there is no current delivered in the rotor. Instead, the coils are fixed around the stator and they do not rotate. The rotor is equipped with permanent magnets [48]. In Figure 2.12, the inside of a BLDC motor can be seen.

Figure 2.12: Inside of a Brushless DC Motor. From [49].

The rotation of the shaft of the motor is achieved by changing the direction of the magnetic fields that are created on the stator coils. By adjusting the magnitude and direction of the current, the rotation can be controlled [48].

This motor operates with high efficiency and can deliver its maximum torque continuously with a wide speed range. Also, due to the lack of brushes, they offer high durability and low noise generation and therefore are mainly used in situations where they are running continuously [48, 49].

For this thesis, this motor is going to be used to model a Radio-controlled (RC) Unmanned Aerial Vehicle (UAV).

2.3.2 Induction Motors vs. Permanent Magnet Synchronous Motors

Unlike the BLDC motor, both the IM and the PMSM run using an Alternating Current (AC) power supply and have, in general, larger dimensions.

In an IM, the stator windings are excited with alternating currents and rotor currents will be produced by induction on the rotor windings that can be made by a set of short-circuited windings or a conducting cage (Squirrel-cage IM - Figure 2.13) or implemented with wound type rotor where the rotor windings are connected through slip rings to an external resistance. It is the most common electric motor in use as they are the most robust and cheap [50].

For a Synchronous Machine (SM), the magnetic field in the rotor can be created either by field windings or by permanent magnets (PMSM). In the first type, brushes are required to apply the external excitation as the field windings are in the rotor. However, for the PMSM the rotor has magnets installed that are responsible for creating the rotor's magnetic field that will interact with the rotating magnetic field created by the alternating currents on the stator side [50]. Figure 2.14 represents a PMSM.

Figure 2.13: "Squirrel Cage" Induction Motor [51].

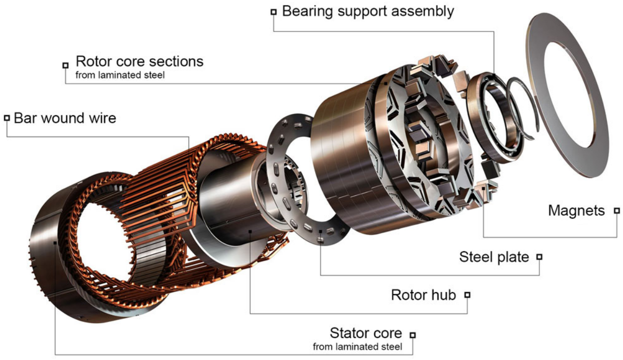

Figure 2.14: Permanent Magnet Synchronous Motor [52].

When considering costs, the PMSM is more expensive due to the high cost of the magnets, however, they operate with higher efficiencies [53]. In addition, PMSM have smaller sizes with more compact models - can be as much as one-third of the IM motor sizes - and have the ability to maintain full torque at low speeds [54].

Table 2.2 includes a comparison between the two models of Electric Motors above-mentioned.

Characteristic	**Induction Motor (IM)**	**PMSM**
Supply	Stator excitation (AC)	Stator excitation (AC)
Speed	Asynchronous mode; Changes with the load	Synchronous mode
Starting	Self-starting	Not self-starting
Efficiency [%]	89.5 - 95	91 - 97
Cost	More robust and cheaper	More expensive due to Permanent Magnets

Table 2.2: Comparison between Induction Motor and Permanent Magnet Synchronous Motor. Adapted from [55].

2.3.3 Cryogenic and Superconducting motors

Due to the high requirements of specific power for aircraft applications, current commercial electric motors still have to be improved to increase the current power density of motors to levels between 10-20 kW/kg. Therefore, one possible solution is using superconducting materials. The electric motors that are currently available are enough for smaller aircraft, however, for passenger-class aircraft, there is a need for higher specific power densities [25].

The main advantage is that superconducting motors can achieve higher power densities (20-30 kW/kg) in smaller and more robust machines with very high efficiencies. However, to achieve the state of superconduction, very low temperatures (ranging from 20K to 90K), and, therefore, cooling systems are required, such as liquid nitrogen or liquid hydrogen. However, this will lead to heavier systems, meaning that more energy is required for the system. Studies performed by NASA for the N3-X concept (mentioned in Section 2.1.3) show that the best cryogenic systems are the ones using Reverse-Brayton Cycle Cryocooler (RBCC) since it does not require their own cold heat exchanger, sharing the total weight and volume with the electric propulsion [25]. Also, the liquid hydrogen with temperatures around 30K that is used in fuel cells (Section 2.2.2) can be used as well as a cooling liquid for the superconducting machine.

However, superconducting motors are not yet available in the market, as there are some technological barriers to overcome.

2.4 Propellers

To make the aircraft move forward, a propeller must be attached to the rotor of the motor in order to create propulsion.

Propellers for aircraft can be made of wood, nylon, fibreglass or carbon fibre whereas wood, fibreglass and carbon fibre are the ones that perform better. There are two important parameters to be selected when choosing a propeller - the diameter and the pitch. The pitch represents the distance that the propeller will move forward in one revolution in a perfect fluid (which air is not). Higher pitches are desirable for high-speed flights and lower pitches make speed control easier. Hence, variable pitch propellers were invented and this allows the pilot to change the pitch of the propeller to give the best thrust characteristics for any given flight condition [56].

The thrust that is created by a rotating propeller is given by

$$F_T = C_T \cdot \rho_{air} \cdot D_p^4 \cdot n^2 \quad \text{[N]} \tag{2.3}$$

where C_T is the thrust coefficient, ρ_{air} is the air density, D_p is the propeller diameter and n is the rotating speed of the propeller in revolutions per second. The thrust coefficient is commonly extracted from experimental data of the propeller [57].

The power required to drive the propeller is given by:

$$P_{in} = C_P \cdot \rho_{air} \cdot D_p^5 \cdot n^3 \quad \text{[W]} \tag{2.4}$$

where C_P is the power coefficient, also extracted from experimental data [58].

To compare different types of propellers, they should all operate under the same advance ratio. Therefore, for a free-stream air speed V, the advance ratio is [58]:

$$J = \frac{V}{n \cdot D_p} \tag{2.5}$$

The propulsive efficiency of a propeller is given by the relation between the input power and the output power:

$$\eta_P = \frac{F_T \cdot V}{P_{in}} = \frac{C_T \cdot J}{C_P} \quad [\%] \tag{2.6}$$

For example, the propeller *APC 12x6E* is used in [59] for a RC aircraft (the same as to be modelled in this thesis). According to the manufacturer [60], its efficiency as a function of the advance ratio and for different rotating speeds of the propeller is given in Figure 2.15.

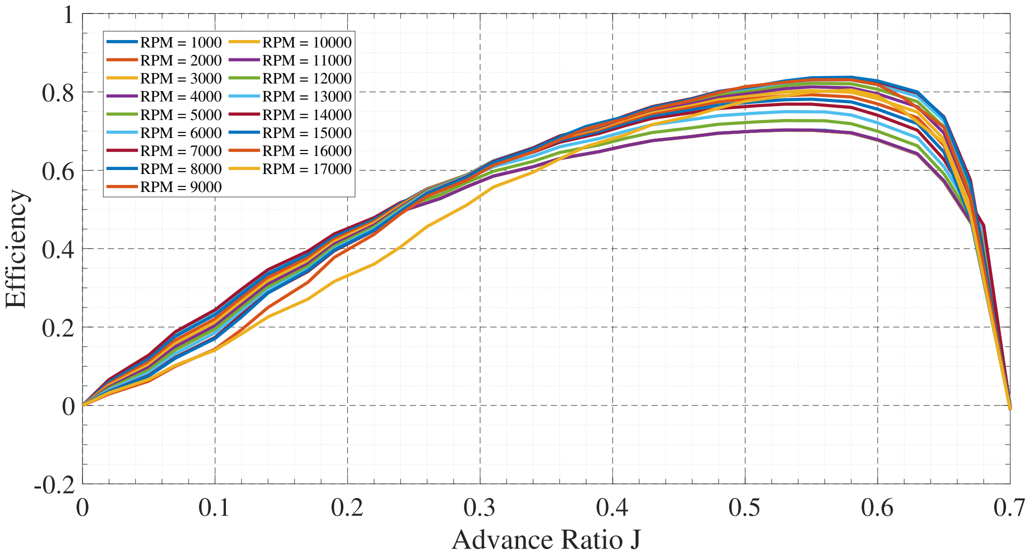

Figure 2.15: Propeller efficiency for different rotating speeds. Adapted from [60].

3

Model of the Systems

Contents

During this thesis, the first step is to develop a generic simulation tool that will be adapted for each aircraft studied so that the energy consumption can be studied. The developed model will be able to simulate a real non-steady flight in a vertical 2D plane. For this, the aircraft will begin its trajectory on the ground, accelerating to a cruising velocity and climbing up to a cruising altitude where it will maintain its trajectory for some time. During this simulation, it is considered that the aircraft will only perform the movement in the X-Z plane. Figure 3.1 illustrates the trajectory that is going to be performed by the models developed ahead.

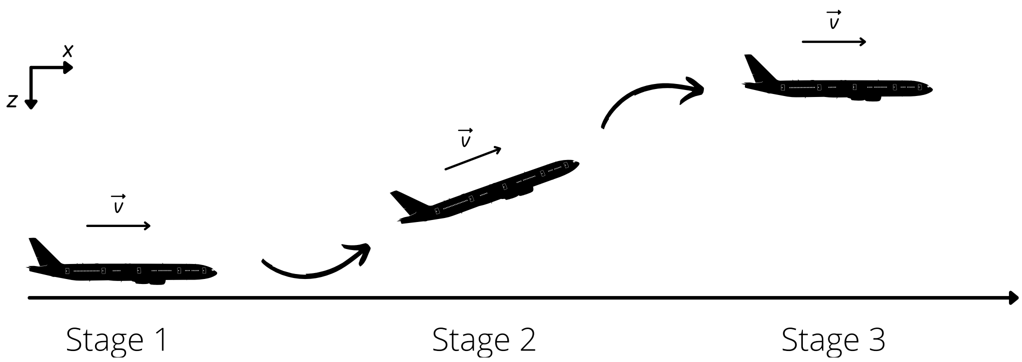

Figure 3.1: Trajectory simulated by the model.

The whole simulation tool can be divided into four main systems that are represented in Figure 3.2 and detailed ahead:

- Aerodynamic Model (Section 3.1) - This block is responsible for computing the thrust that the aircraft needs to be able to follow the trajectory and velocity profile;
- Propeller Model (Section 3.2) - Here, with the force required by the aircraft, the mechanical power and rotational speed are computed.
- Electric Motors Model (Section 3.3) - With the given rotational speed and mechanical power required by the propeller, the electrical power needed to feed the electric motor is computed.
- Energy Storage Systems Model (Section 3.4) - In this block, the total energy that has to be stored is computed, with the electric power required by the electric motor.

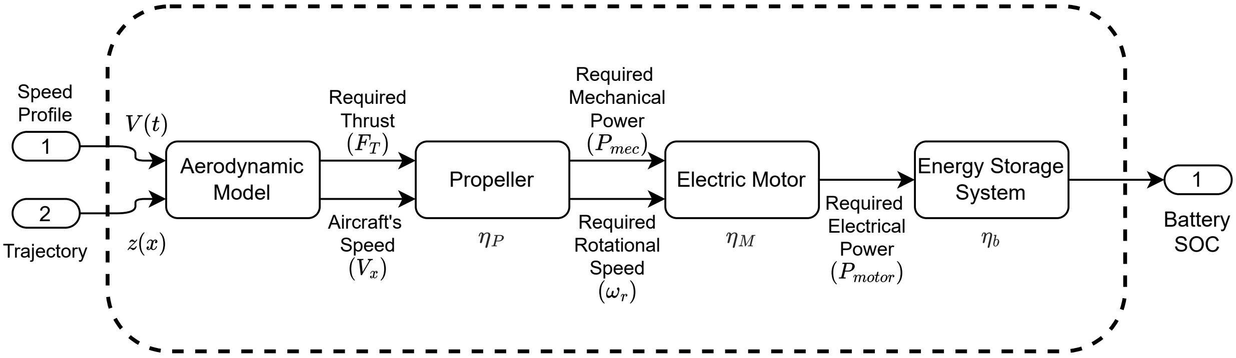

Figure 3.2: Overall block diagram.

3.1 Aerodynamic Model

To derive the dynamic equations of motion for this flight trajectory, the following physical model assumptions are going to be used [61]:

- The earth is flat, non-rotating and considered as an approximate inertial referential, the so-called *flat earth model*. The gravity acceleration is constant and perpendicular to the surface of the earth.
- The atmosphere is considered to be at rest relative to the earth and the atmospheric properties are only functions of altitude.
- The aircraft has fixed engines with an aft tail and right-left aircraft of symmetry.
- The only forces acting on the aircraft are the thrust, aerodynamic forces and weight and they all act on the centre of gravity of the aircraft.

3.1.1 Coordinate axis systems

In the aeronautical field, it is common to use more than one referential to represent the forces as it makes some computations easier. There are four coordinate systems used [59, 61]:

- **Ground axis system** (xyz) - Fixed to the surface of the Earth at mean sea level. xz aircraft is the vertical plane, z is positive downwards and x and y follow the right-hand rule.
- **Local horizon axis system** $(x_h y_h z_h)$ - Moves with the aircraft but their axis remain parallel to the ground.
- **Wind axis system** $(x_w y_w z_w)$ - Moves with the aircraft and the x_w axis is coincident with the velocity vector and positive in the forward direction. y_w is orthogonal with x_w from the clockwise direction and z_w points downwards in the vertical axis of the aircraft.

- **Body axis system** $(x_b y_b z_b)$ - Fixed to the aircraft where x_b is the axis where the aircraft's nose points, y_b is orthogonal to the x_b parallel with the lateral axis and z_b is orthogonal to both x_b and y_b pointing downwards.

The Figure 3.3 represents the above-mentioned coordinate axis where $\vec{i}$, $\vec{j}$ and $\vec{k}$ represent the unit vectors for axis x, y and z respectively.

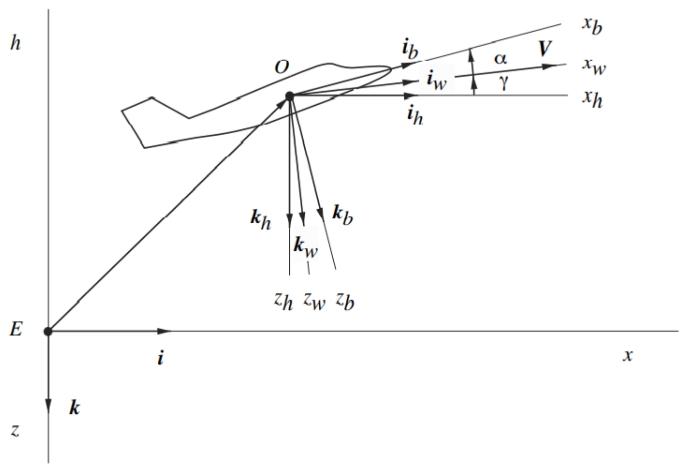

Figure 3.3: Coordinate systems for Flight in a Vertical 2D X-Z Plane [61].

3.1.1.A Aircraft Rotation Axis

The rotations that the aircraft can do are along three axis - Yaw, Pitch and Roll. They represent the rotations around the z, y and x axis respectively. These three axes of rotations can be seen in Figure 3.4. In this thesis, only a pitch rotation is considered.

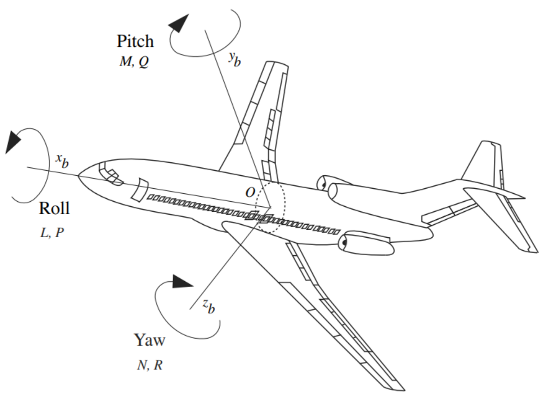

Figure 3.4: Yaw, Pitch and Roll rotation axis [61].

3.1.1.B Angles

To describe the aircraft's trajectory, five angles can be defined:

- **Heading Angle** (β) - Angle between the north and the horizontal component of the velocity vector. Describes which direction the aircraft is moving relative to cardinal directions. This is not considered in this model, because the aircraft will only perform movement in the X-Z plane.

- **Bank Angle** (μ) - Represents a rotation of the lift force around the velocity vector. Indicates whether the aircraft is turning. In this simulation, the angle is zero since it is considered that the aircraft does not turn.

- **Flight Path Angle** (γ) - Angle between horizontal and the velocity vector. Describes whether the aircraft is climbing or descending.

- **Angle of Attack** (α) - Angle between the wind $x_w y_w$-plane and the aircraft longitudinal axis. Determines the magnitude of the force of lift.

- **Pitch Angle** (θ) - Angle between the aircraft's longitudinal axis and horizontal horizon plane. It is the sum of the Flight Path Angle and the Angle of Attack:

$$\theta = \gamma + \alpha \tag{3.1}$$

The angles α and γ can be seen in Figure 3.3, so as θ that is the sum of the previous two. Angle β can be perceived in Figure 3.5 and the angle μ in Figure 3.6

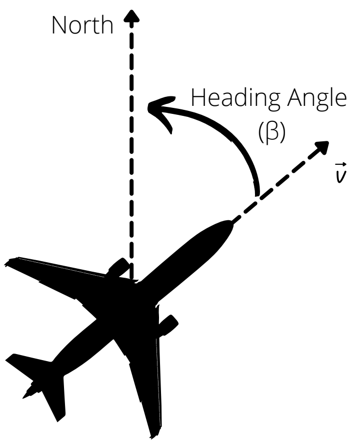

Figure 3.5: Heading Angle.

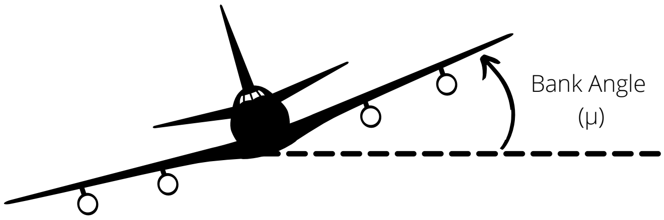

Figure 3.6: Bank Angle.

3.1.2 Forces acting on an aircraft

Before studying the dynamics of the aircraft, the forces acting on it should be analysed and defined. During the flight, the aircraft is exposed to Thrust ($\overrightarrow{F_T}$), Aerodynamic Forces ($\vec{A}$) and its Weight ($\overrightarrow{W}$). Thus, the resultant external forces can be written:

$$\overrightarrow{F_r} = \overrightarrow{F_T} + \vec{A} + \overrightarrow{W} \quad \text{[N]} \tag{3.2}$$

The Aerodynamic Forces can be decomposed in parallel and perpendicular components to the velocity vector. The parallel component is the Drag ($\vec{D}$) and the perpendicular component is the Lift ($\vec{L}$):

$$\vec{A} = \vec{D} + \vec{L} \quad \text{[N]} \tag{3.3}$$

Drag is the aerodynamic force that opposes the aircraft's motions through the air. This non-desirable force results from the interaction between the aircraft and the fluid around it (air) when the object and the fluid have different velocities. Lift is the force generated by the wings that holds the aircraft in the air. This force is generated when a flow of a fluid is turned by a solid object. The airflow is turned in one direction and, according to Newton's Third Law (Action and Reaction), the lifting force is generated in the opposite direction. Figure 3.7 represents the mentioned forces acting on an aircraft during flight.

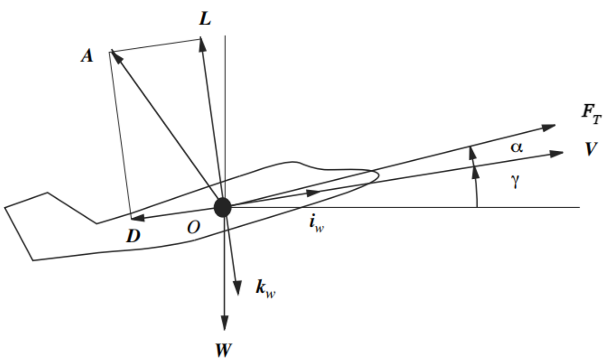

Figure 3.7: Forces acting on an aircraft during flight. Adapted from [61].

It is noted that before the take-off, when the aircraft is on the ground, there is an extra force - the Normal Reaction Force ($\vec{N}$) - that is perpendicular to the surface with the same value as the Weight, and opposing direction.

3.1.3 Dynamic Equations of Motion

To derive the equations of motion, a more direct deviation can be achieved by using the wind referential, since, in this case, the velocity has only one component, whereas in the horizon referential it has two components:

$$\vec{V} = V\,\vec{i_w} = V\cos\gamma\,\vec{i_h} - V\sin\gamma\,\vec{k_h} \quad \text{[m/s]} \tag{3.4}$$

In the wind referential, the forces can be written as:

$$\vec{F_T} = F_T\cos\alpha\,\vec{i_w} - F_T\sin\alpha\,\vec{k_w} \quad \text{[N]} \tag{3.5}$$

$$\vec{D} = -D\,\vec{i_w} \quad \text{[N]} \tag{3.6}$$

$$\vec{L} = L\sin\mu\,\vec{j_w} - L\cos\mu\,\vec{k_w} \quad \text{[N]} \tag{3.7}$$

$$\vec{W} = -W\sin\gamma\,\vec{i_w} + W\cos\gamma\,\vec{k_w} \quad \text{[N]} \tag{3.8}$$

Therefore, the resultant external forces as seen in Equation (3.2) becomes:

$$\vec{F_r} = (F_T\cos\alpha - D - W\sin\gamma)\ \vec{i_w} + (L\sin\mu)\ \vec{j_w} - (F_T\sin\alpha + L\cos\mu - W\cos\gamma)\ \vec{k_w} \quad \text{[N]} \tag{3.9}$$

For simplicity, it was not considered the Normal Force while the aircraft is on the ground. Instead, the simulations start at the point where the aircraft leaves the ground and starts climbing to cruising altitude. This way, the aircraft has already an initial velocity and a thrust being applied, thus, generating lift.

Before computing the magnitudes of the forces, an important concept to be defined is the Dynamic Pressure (q) which refers to the pressure of air moving over the aircraft. It is given as follows:

$$q = \frac{1}{2}\cdot\rho_{air}\cdot V^2 \quad \text{[Pa]} \tag{3.10}$$

where ρ_{air} is the air density, and V is the magnitude of the velocity of the aircraft.

The Drag, Lift and Weight magnitudes are computed with the following expressions, respectively:

$$D = C_D\cdot q\cdot S \quad \text{[N]} \tag{3.11}$$

$$L = C_L\cdot q\cdot S \quad \text{[N]} \tag{3.12}$$

$$W = M\cdot g \quad \text{[N]} \tag{3.13}$$

where C_D and C_L are the non-dimensional drag and lift coefficients, q is the dynamic pressure and S is the wing area of the aircraft. The Lift coefficient only depends on the wing configuration and on the Angle of Attack (α). However, the Drag coefficient has an additional dependency on the velocity: the higher the velocity is, the lower the coefficient of drag will be. This way, for a more detailed model implementation, the Drag coefficient can be divided into two independent components: C_{D0} that is velocity dependent and C_{Di} that is only dependent on the Angle of Attack (α).

$$C_L = f(\alpha) \qquad\qquad C_D = f(\alpha, V) = C_{D0}(V) + C_{Di}(\alpha) \tag{3.14}$$

For the weight magnitude, M is the total mass of the aircraft and g is the gravitational acceleration considered constant and equal to 9.8 m/s^2.

The Thrust magnitude and the aircraft's Angle of Attack (α) will result from a closed-loop control system with Proportional, Integral and Derivative (PID) controllers and negative feedback. The Flight Path Angle (γ) is calculated with a feedback system without control. All these calculations are detailed ahead in Section 3.1.4.

After computing the resultant forces, by making use of Newton's Second Law, it is possible to compute the acceleration:

$$\overrightarrow{F_r} = M \cdot \vec{a} \quad \text{[N]} \tag{3.15}$$

From the acceleration, the velocity and the position of the aircraft become direct:

$$V = \int a \cdot dt + V_0 \tag{3.16}$$

$$x = \int V_x \cdot dt + x_0 \qquad\qquad z = \int V_z \cdot dt + z_0 \tag{3.17}$$

To compute the mechanical power and respective energy that the propeller has to provide, the following equations are used:

$$P_{aero} = \overrightarrow{F_T} \cdot \vec{V} = \sqrt{[(F_T \cdot \cos\alpha) \cdot V_x]^2 + [(-F_T \cdot \sin\alpha) \cdot V_z]^2} \quad \text{[W]} \tag{3.18}$$

$$E_{aero} = \int P \cdot dt \quad \text{[J]} \tag{3.19}$$

As seen previously, all forces are computed in the wind referential axis. Even though this referential makes the computations easier, it is not very intuitive to analyse the results. Hence, to convert the forces to the local horizon axis system the conversion matrix in Equation (3.20) will be used [61].

$$\begin{bmatrix} i_h \\ j_h \\ k_h \end{bmatrix} = \begin{bmatrix} \cos\gamma\cos\beta & \sin\mu\sin\gamma\cos\beta - \cos\mu\sin\beta & \cos\mu\sin\gamma\cos\beta + \sin\mu\sin\beta \\ \sin\beta\cos\gamma & \sin\mu\sin\gamma\sin\beta + \cos\mu\cos\beta & \cos\mu\sin\gamma\sin\beta - \sin\mu\cos\beta \\ -\sin\gamma & \cos\gamma\sin\mu & \cos\mu\cos\gamma \end{bmatrix} \begin{bmatrix} i_w \\ j_w \\ k_w \end{bmatrix} \tag{3.20}$$

The previous conversion matrix will also be used to compute the position of the aircraft in the Local Horizon referential, by first converting the speed to this referential and then integrating it to get the position.

This subsystem is represented graphically in Figure 3.8 with the respective equations used in each step. These systems take as inputs the desired trajectory to be followed by the aircraft as well as the velocity profile. The three feedback control systems are going to be detailed ahead in Section 3.1.4.

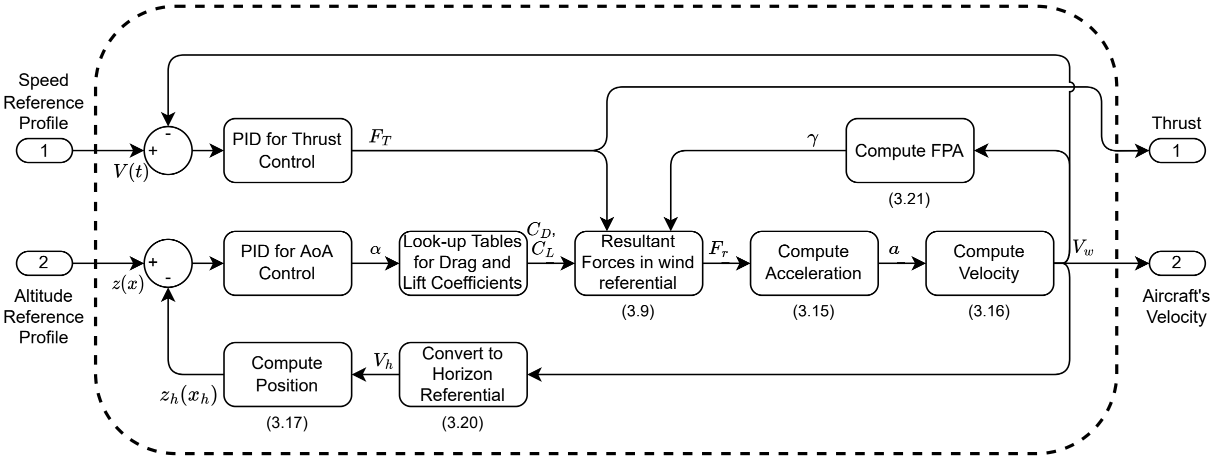

Figure 3.8: Representation of the subsystem Aerodynamic Model.

3.1.4 Closed-loop Control System

Two closed-loop control systems with negative feedback were implemented to control the desired altitude and velocity profiles.

3.1.4.A Altitude control

For the altitude loop, the reference was set as the desired altitude (z) as a function of the longitudinal coordinate of the aircraft (x). Based on the current position of the aircraft (x), the current altitude (z) is compared with the desired one and this difference will be the input of a PID controller, therefore controlling the Angle of Attack (α).

If the aircraft's altitude is above the reference, the difference will be negative and therefore the PID will reduce its output (the Angle of Attack) so that the aircraft lowers its nose and gets closer to the reference. On the other side, if the altitude of the aircraft is below the reference, the difference will be positive and the PID will increase its output as a way to raise the aircraft's nose and increase the altitude.

3.1.4.B Velocity control

The velocity control is very similar to the altitude control mentioned in Section 3.1.4.A. However, the reference is set as a function of time (t). In this case, the difference between the actual velocity of the aircraft and the desired one will be the input of the PID. The output will be the thrust applied to the aircraft.

If the aircraft's velocity is above the reference, the difference will be negative, leading the PID to decrease its output (the Thrust), getting its velocity closer to the reference. On the other hand, if the velocity of the aircraft is below the reference, the difference will be positive, making the PID increase its output, applying more force to increase the velocity.

3.1.4.C Flight Path Angle control

By using the wind referential, the velocity has only one component - under the i_w axis. This axis is constantly changing accordingly to the velocity vector. Therefore, the velocities under the j_w and k_w axes are zero. However, during the flight, the aircraft changes its movement direction, for example, when it is climbing up during the takeoff. Therefore, while the aircraft does not present any velocity on the j_w and k_w axes, these axes are changing due to the control of the Angle of Attack.

The change of the Flight Path Angle, which defines the change of wind reference, can be made through equation Equation (3.21), where i is the time instant. At a given time instant, i, for a fixed wind reference, the balance of forces results in a new direction of aircraft (V_x, V_z). Thus, the new wind reference, $\gamma^{(i+1)}$, can be computed.

$$\gamma^{(i+1)} = \arctan\left(\frac{V_z^{(i)}}{V_x^{(i)}}\right) \tag{3.21}$$

3.2 Propeller Model

The rotation of the propeller is responsible for creating the propulsive force that makes the aircraft move - the Thrust. It will take as inputs the linear velocity of the aircraft and the thrust required by it. As outputs, it will calculate the rotational velocity of the propeller and the mechanical power that has to be available in the motor's shaft. Figure 3.9 represents a diagram of this subsystem.

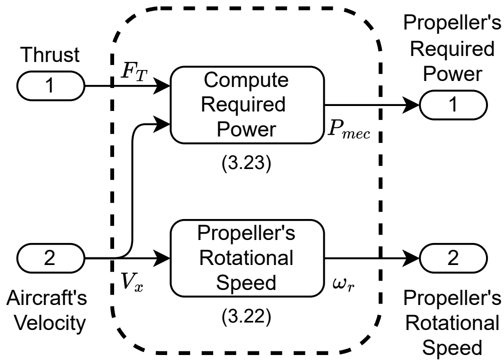

Figure 3.9: Representation of the subsystem Propeller.

To model the propeller, it was considered that it was always working on the optimal advance ratio point (J_{opt}), which corresponds to the highest efficiency point (η_{opt}). This can be done by regulating the blades' pitch.

By rearranging the Equation (2.5), it is possible to calculate the rotational speed (ω_r), given the advance ratio (J), the linear speed of the aircraft under the x_w axis (V_{xw}) and the diameter of the propeller (D_p):

$$\omega_r = \frac{V}{J \cdot D_p} \cdot 2\pi \quad \text{[rad/s]} \tag{3.22}$$

To calculate the mechanical power required to run the propeller, Equation (2.6) can be rearranged in the following expression:

$$P_{mec} = \frac{F_T \cdot V}{\eta_P} \quad \text{[W]} \tag{3.23}$$

3.3 Electric Motors Model

The electric motor follows the propeller and is responsible for providing mechanical power through the rotation of its shaft. As inputs, it will take the rotational velocity of the shaft (ω_r) and the required mechanical power (P_{mec}) in order to calculate the electric power necessary to feed the motor.

For this purpose, two electric motors were designed - A BLDC motor in Section 3.3.1 and a PMSM in Section 3.3.2.

3.3.1 Model of the Brushless DC Motor

One of the simulated aircraft is an RC UAV which uses a BLDC motor. It is a very small motor given the small dimensions of the aircraft as well. A graphical representation of this subsystem can be seen in Figure 3.10 with the respective equations used for each calculation.

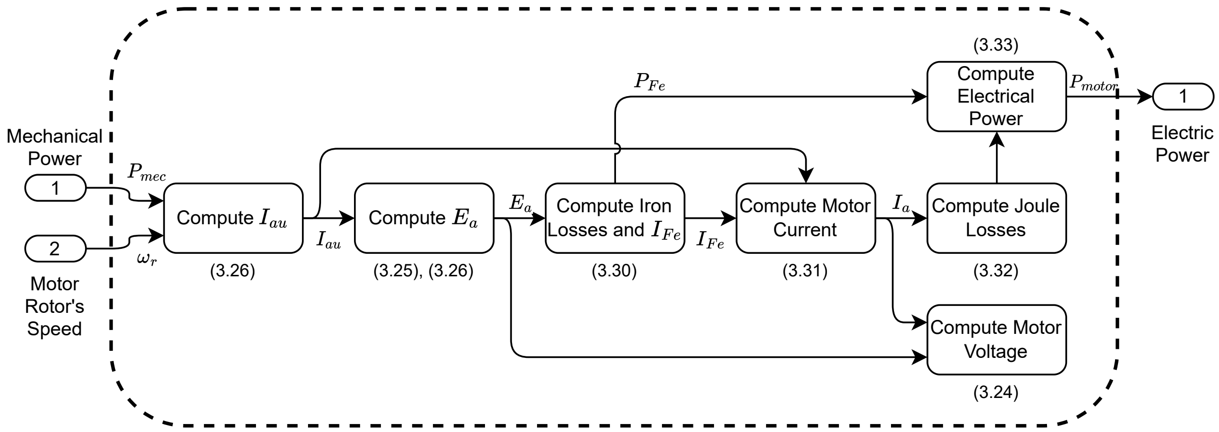

Figure 3.10: Representation of the subsystem Electric Motor - BLDC.

First of all, it is important to take a look at the equivalent circuit of this motor, to easily dive into the equations. This circuit can be seen in Figure 3.11.

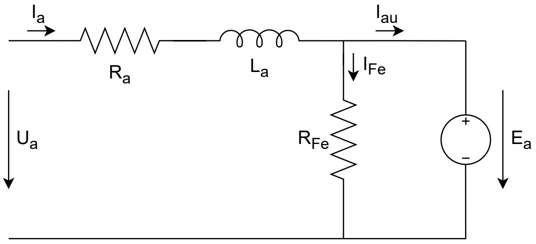

Figure 3.11: Equivalent Circuit of the Brushless DC Motor.

By applying Kirchhoff's Law in the circuit of Figure 3.11, the following equation can be derived:

$$U_a = R_a I_a + L_a \frac{dI_a}{dt} + E_a \quad \text{[V]} \tag{3.24}$$

where the derivative term can be neglected, as the changes in the electrical quantities happen in long intervals of time, leading the derivative to zero.

For this type of motor, there is an important relationship between the voltage source E_a and the rotational velocity of the rotor (ω_r) represented by K_ϕ:

$$E_a = K_\phi \cdot \omega_r \quad \text{[V]} \tag{3.25}$$

Also, for the output torque (T_e):

$$T_e = K_\phi \cdot I_{au} = \frac{P_{mec}}{\omega_r} \quad \text{[N.m]} \tag{3.26}$$

The current I_{au} can be computed by using Equation (3.26) and knowing the constant K_ϕ, the Mechanical Power P_{mec} and the rotational velocity ω_r.

Then, the equation of the mechanical power can also be computed:

$$P_{mec} = E_a \cdot I_{au} \quad \text{[W]} \tag{3.27}$$

From Equation (3.27) and knowing I_{au}, the voltage E_a can be computed.

The next step is to calculate the current I_{Fe}. For this, the iron losses (P_{Fe}) are going to be computed from the no-load condition and considered to be constant.

In this operation mode, the following conditions are met:

$$P_{mec} = 0 = E_a \cdot I_{au} = 0 \Longrightarrow I_{au} = 0 \Longrightarrow T_e = K_\phi \cdot I_{au} = 0 \tag{3.28}$$

By considering the nominal voltage (U_N) the same as the no-load voltage (U_0), the input power can be written as:

$$P^0_{motor} = U_N \cdot I_0 = P_{Fe} + P_J \quad \text{[W]} \tag{3.29}$$

The iron losses P_{Fe} can be computed from Equation (3.30). With the first equality, the value of P_{Fe} is obtained, and the iron current I_{Fe} is computed with the second equality.

$$P_{Fe} = \frac{E_a^2}{R_{Fe}} = E_a \cdot I_{Fe} \quad \text{[W]} \tag{3.30}$$

Then, the total motor current I_a is computed as the sum of the previous two calculated:

$$I_a = I_{Fe} + I_{au} \quad \text{[A]} \tag{3.31}$$

Now, the Joule losses (P_J) can be computed with:

$$P_J = R_a \cdot I_a^2 \quad \text{[W]} \tag{3.32}$$

Now, all the variables are known and it is now possible to compute the input voltage U_a with Equation (3.24).

The total electric input power can be computed with the following equation:

$$P_{motor} = U_a \cdot I_a = P_{Fe} + P_J + P_{mec} \quad \text{[W]} \tag{3.33}$$

The motor's efficiency is useful to analyse its operation and can be calculated with:

$$\eta_M = \frac{P_{mec}}{P_{motor}} \quad [\%] \tag{3.34}$$

3.3.2 Model of the Permanent Magnet Synchronous Motor

Now, a PMSM will be used to simulate the two-passenger aircraft. To control this motor, Field Oriented Control (FOC) will be used. Figure 3.12 contains a schematic of the implementation of this subsystem where for each block the equations used can also be seen.

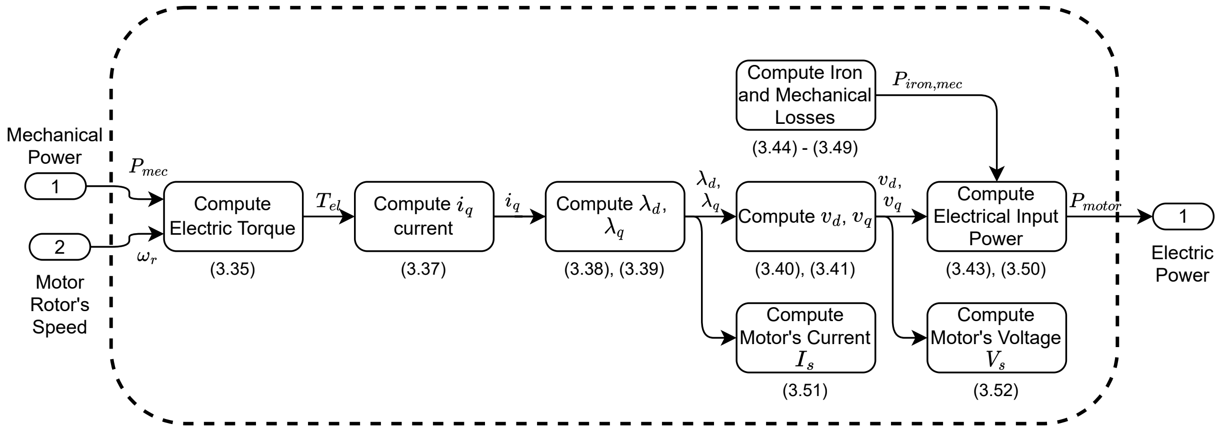

Figure 3.12: Representation of the subsystem Electric Motor - PMSM.

From the mechanical power required by the propeller and the rotational velocity, the torque required at the motor's shaft can be computed:

$$T_e = \frac{P_{mec}}{\omega_r} \quad \text{[N.m]} \tag{3.35}$$

With this technique, the RMS voltage and current of the motor are calculated from the equivalent DC direct and quadrature voltages (v_d, v_q) and currents (i_d, i_q), respectively. This is a space-vector control technique where the direct axis current is always zero, since its axis is aligned with the rotor flux:

$$i_d = 0 \quad \text{[A]} \tag{3.36}$$

From the electrical torque, the quadrature current (i_q) can be computed:

$$T_e = \frac{3}{2} n_{pp} \left[(L_d - L_q)\, i_d + \lambda_{PM} \right] \overset{(i_d=0)}{\Leftrightarrow} i_q = \frac{T_e}{\frac{3}{2} n_{pp} \lambda_{PM}} \quad \text{[A]} \tag{3.37}$$

where n_{pp} is the number of pole pairs of the PMSM, L_d and L_q are the direct and quadrature axis inductances and λ_{PM} is the magnetic flux of the rotor's permanent magnets.

The next step is to calculate the direct and quadrature fluxes (λ_d, λ_q):

$$\lambda_d = L_d i_d + \lambda_{PM} \overset{(i_d=0)}{=} \lambda_{PM} \quad \text{[Wb]} \tag{3.38}$$

$$\lambda_q = L_q i_q \quad \text{[Wb]} \tag{3.39}$$

With the fluxes, the direct and quadrature voltages (v_d, v_q) can be computed:

$$v_d = R_s i_d + \frac{d\lambda_d}{dt} - \omega_{me} \lambda_q \quad \text{[V]} \tag{3.40}$$

$$v_q = R_s i_q + \frac{d\lambda_q}{dt} + \omega_{me}\lambda_d \quad \text{[V]} \tag{3.41}$$

where R_s is the stator resistance and ω_{me} is the electro-mechanical angular velocity, computed as follows:

$$\omega_{me} = n_{pp} \cdot \omega_s = n_{pp} \cdot \omega_r \quad \text{[rad/s]} \tag{3.42}$$

With all the equivalent voltages and currents computed, the electric input power can be computed:

$$P_e = \frac{3}{2}\left[v_d \cdot i_d + v_q \cdot i_q\right] \overset{(i_d=0)}{=} \frac{3}{2} v_q i_q \quad \text{[W]} \tag{3.43}$$

However, this model does not simulate iron and mechanical losses that have to be included in the electrical power required to supply the motor. The iron losses can be split into hysteresis losses and Eddy's current losses. The first is directly proportional to the magnetic flux density B and to the square of the frequency f, whereas the second is proportional to both the squares of the magnetic field and frequency:

$$P_{iron,loss} = P_{hyst} + P_{eddy} = k_h \cdot B^2 \cdot f + k_e \cdot B^2 \cdot f^2 \quad \text{[W]} \tag{3.44}$$

The Eddy currents can be neglected when compared to the hysteresis losses. Also, the magnetic field in PMSM is fixed and equal to the permanent magnets flux λ_{PM}. Thus, Equation (3.44) can be simplified into:

$$P_{iron,loss} = k_h \cdot B^2 \cdot f = k_h \cdot \lambda_{PM}^2 \cdot f \propto a \cdot \omega_r \quad \text{[W]} \tag{3.45}$$

Regarding the mechanical losses, they can be derived from viscous torque (T_{visc}) that is proportional to the rotor's rotational speed (ω_r):

$$T_{visc} = b \cdot \omega_r \quad \text{[Nm]} \tag{3.46}$$

To compute the power associated with this torque, it should be multiplied by the rotor's rotational speed:

$$P_{mec,loss} = T_{visc} \cdot \omega_r = b \cdot \omega_r^2 \quad \text{[W]} \tag{3.47}$$

Furthermore, the iron and mechanical losses will be estimated considering that the no-load power is equal to the sum of iron and mechanical losses:

$$P_{motor}^0 = P_{iron,mec} = P_{iron,loss} + P_{mec,loss} = a \cdot \omega_r + b \cdot \omega_r^2 \quad \text{[W]} \tag{3.48}$$

The constants a and b can be computed from the no-load power. By knowing the losses (P_0) and the rotational velocity of the rotor (ω_r^0) under this condition, the iron and mechanical losses can be computed. However, due to the lack of information from the manufacturer, for the considered PMSM a contribution of 80% to the iron losses and 20% to the mechanical losses was considered [62]:

$$P^0_{iron,loss} = 0.8P_0 = a \cdot \omega^0_r \quad \text{[W]} \qquad\qquad P^0_{mec,loss} = 0.2P_0 = b \cdot \left(\omega^0_r\right)^2 \quad \text{[W]} \tag{3.49}$$

Now, with the estimation of the losses, the total electric input power required can be computed:

$$P_{motor} = P_e + P_{iron,mec} \quad \text{[W]} \tag{3.50}$$

The AC voltage and current necessary to feed the motor can also be computed with the following equations, where I_s is the *RMS* value of the stator current and V_s is the phase-to-phase *RMS* value of the stator voltage:

$$I_s = \frac{\sqrt{i_d^2 + i_q^2}}{\sqrt{2}} \quad \text{[A]} \tag{3.51}$$

$$V_s = \frac{\sqrt{3} \cdot \sqrt{v_d^2 + v_q^2}}{\sqrt{2}} \quad \text{[V]} \tag{3.52}$$

To better analyse the operation of the motor, its efficiency can be computed with:

$$\eta_M = \frac{P_{mec}}{P_{motor}} \quad [\%] \tag{3.53}$$

3.4 Energy Storage Systems Model

To feed the electric motor with the required power, a battery system is mandatory. On top of that, some additional equipment is necessary like converters, rectifiers or even transformers, and their efficiency should be considered.

So, the power demanded by the batteries (P_{bat}) will be slightly higher than the one required by the electric motor (P_{motor}), due to the efficiency of the system (η_b) that includes the electronic equipment ($\eta_{e.e.}$) and the battery itself (η_{bat}):

$$P_{bat} = \frac{P_{motor}}{\eta_b} = \frac{P_{motor}}{\eta_{e.e.} \times \eta_{bat}} \quad \text{[W]} \tag{3.54}$$

With the total capacity of the battery known (E_{full}), it is possible to calculate the State of Charge (SOC) for each time instant (t):

$$SOC(t) = E_{full} - \int_0^t P_{bat} \cdot dt \quad \text{[Wh]} \tag{3.55}$$

As a safety measure, the simulation will stop automatically when the SOC reaches 20% of the total capacity of the battery.

In Figure 3.13 a schematic representation of the implementation of this subsystem can be seen, as well as the respective equations used for each step.

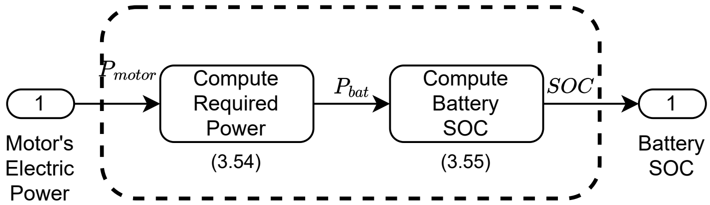

Figure 3.13: Representation of the subsystem ESS.

4

Results

Contents

In this chapter, the required data for the implementation of the models will be detailed followed by the respective results for each of the implemented models. The structure explained in Chapter 3 is common between all the models, just adapted to the specifications of each of them.

There are going to be implemented 3 aircraft models - a RC UAV in Section 4.1, a two-passenger full-electric aircraft in Section 4.2 and in the last place, in Section 4.3, a fuel-powered aircraft is converted into an AEA.

4.1 Case study for a RC UAV

As the first case study for this thesis, a model for an UAV was built in order to evaluate the energy consumption of the aircraft propulsion system. This includes the power required to run the motor as well as the energy to be stored in the batteries. This model will be based on the RC aircraft shown in Figure 4.1.

This aircraft is sold in pieces to be assembled together. It comes with a fuel engine but also has the option to fly with an electric motor.

Figure 4.1: Avistar Elite .46-55 GP/EP 62.5" ARF [63].

4.1.1 Data required to simulate the model

The data required to simulate the model is presented in the next tables, categorized by each subsystem in the simulation tool.

4.1.1.A Aerodynamic Model

The first subsystem is the Aerodynamic Model. The Table 4.1 contains the data required for this block.

Data for the Aerodynamic Model			
Name	**Symbol**	**Unit**	**Value**
Model name	-	-	Avistar Elite .46-55 GP/EP 62.5” ARF
Wingspan	-	m	1.590
Length	-	m	1.395
Mass	$M_{aircraft}$	kg	3.0
Wing Area	S	m^2	0.433
Lift Coefficient	$C_L(\alpha)$	-	Figure 4.2
Drag Coefficients	$C_{D0}(V)$, $C_{Di}(\alpha)$	-	Figures 4.3 and 4.4
Speed Profile	$V(t)$	m/s	Figure 4.5
Trajectory Profile	$z(x)$	m	Figure 4.6

Table 4.1: Data required for the Aerodynamic Model of the RC UAV. Adapted from [59, 63]

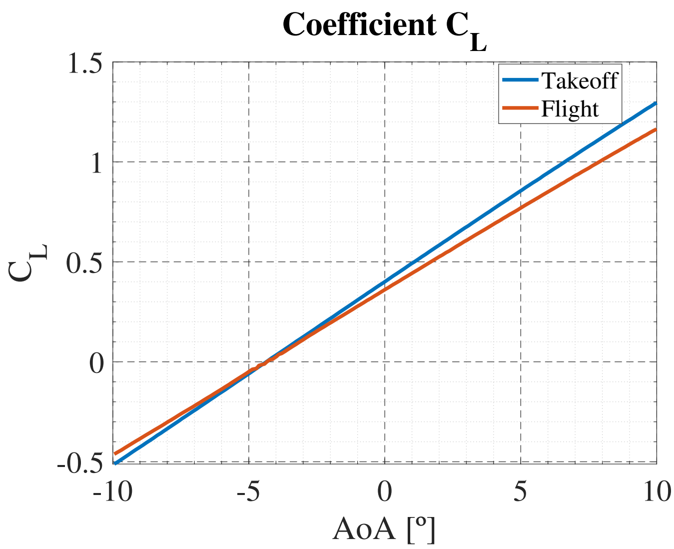

Figure 4.2: Lift coefficient C_L for the RC UAV model. Adapted from [59].

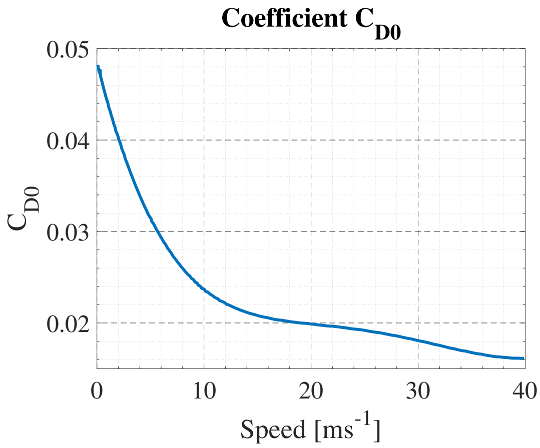

Figure 4.3: Drag coefficient C_{D0} for the RC UAV model. Adapted from [59].

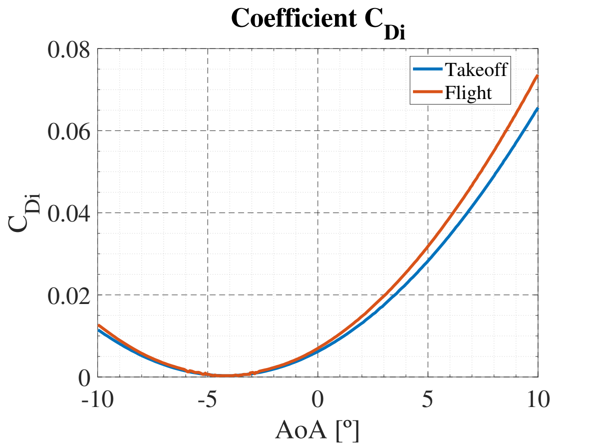

Figure 4.4: Drag coefficient C_{Di} for the RC UAV model. Adapted from [59].

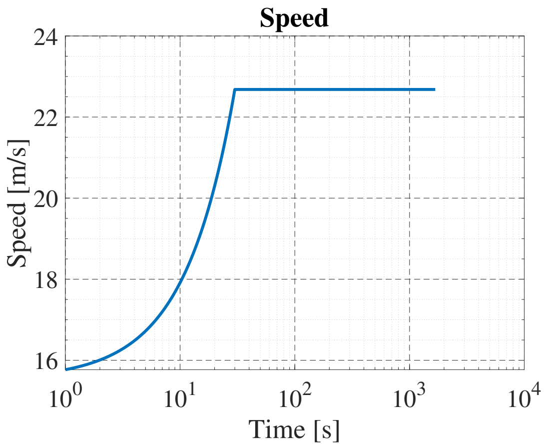

Figure 4.5: Speed profile for the RC UAV model. Adapted from [59].

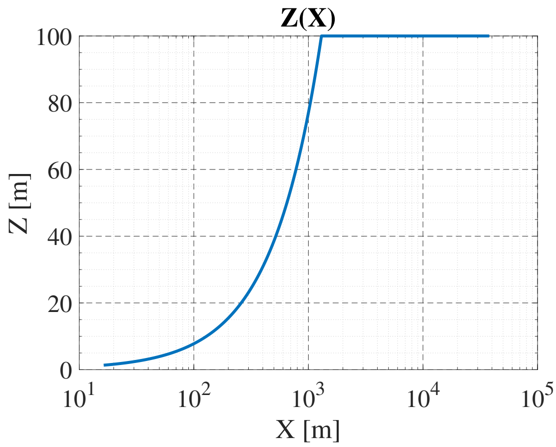

Figure 4.6: Altitude profile for the RC UAV model. Adapted from [59].

4.1.1.B Propeller Model

In Table 4.2, the data required to run the Propeller Model is shown.

Data for the Propeller Model			
Name	**Symbol**	**Unit**	**Value**
Model name	-	-	APC 12x6E
Number of Blades	-	-	2
Mass	$M_{propeller}$	g	45.93
Diameter	D_p	m	0.3048
Optimal Advance Ratio	J_{opt}	-	0.55
Efficiency	η_p	%	Figure 2.15

Table 4.2: Data required for the Propeller Model of the RC UAV. Adapted from [60].

4.1.1.C BLDC Motor Model

Table 4.3 contains the data required to run the BLDC Motor Model.

Data for the BLDC Motor Model			
Name	**Symbol**	**Unit**	**Value**
Model name	-	-	RimFire .46 (42-60-800)
Motor type	-	-	BLDC
Mass	M_{motor}	g	268
Diameter	-	mm	42
Length	-	mm	60
Nominal Voltage	U_N	V	20
Maximum Current (DC)	I_{max}	A	60
No-load Current	I_0	A	4.6
Speed-Voltage Constant	K_ϕ	rpm/V	800
Internal Resistance	R_a	Ω	0.04
Iron Resistance	R_{Fe}	Ω	4.32

Table 4.3: Data required for the BLDC Motor Model of the RC UAV. Adapted from [59, 64].

4.1.1.D Battery Model

In Table 4.4, the data required for the LiPo Battery Model is detailed.

Data for the LiPo Battery Model			
Name	**Symbol**	**Unit**	**Value**
Battery Type	-	-	LiPo
Mass	M_{bat}	g	524
Length	-	mm	138
Width	-	mm	47
Height	-	mm	48
Nominal Voltage	U_N	V	14.8
Storage Capacity	E_{full}	mAh	5400
Electronic Equipment Efficiency	$\eta_{e.e}$	$\%$	95
Battery Efficiency	η_{bat}	$\%$	95

Table 4.4: Data required for the LiPo Battery Model of the RC UAV. Adapted from [65, 66].

4.1.2 Simulation Results

With the data specified in Section 4.1.1, the model was simulated and the results are shown ahead.

In Figure 4.7 the aircraft's speed with the respective reference is presented. Figure 4.8 shows the trajectory followed by the aircraft, as well as its reference.

In Figures 4.9 and 4.10 the power and energy consumption for each system individually can be seen.

With respect to the last subsystem, Figure 4.11 contains the Battery's SOC over the simulation's time.

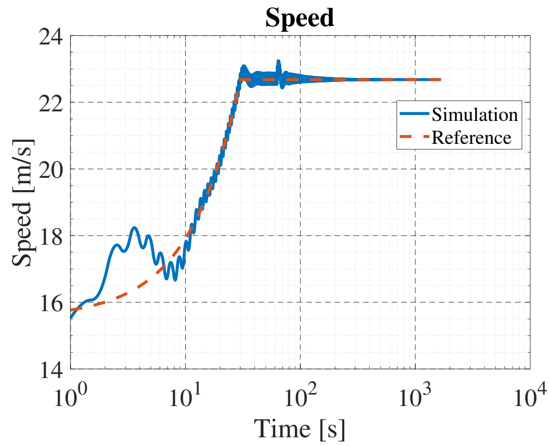

Figure 4.7: Speed performed by the RC UAV model.

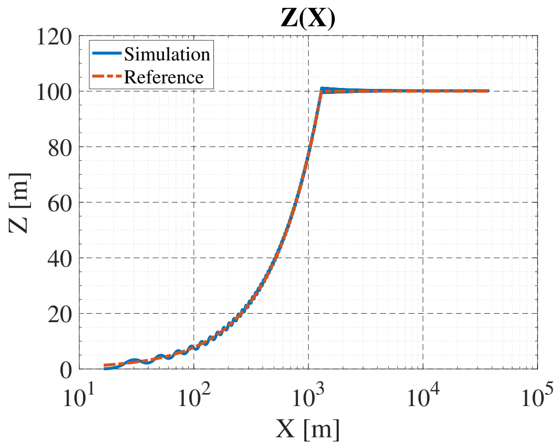

Figure 4.8: Trajectory followed by the RC UAV model.

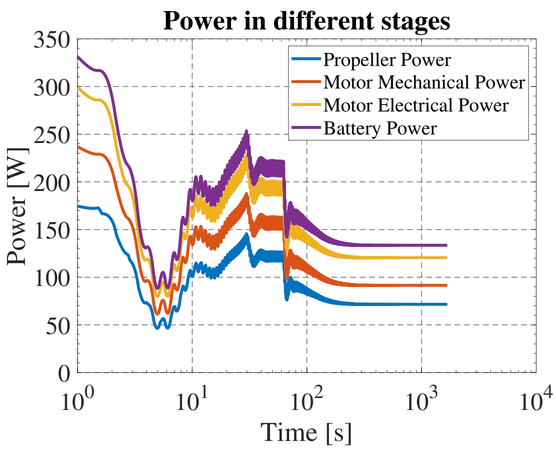

Figure 4.9: Power consumption by the RC UAV model.

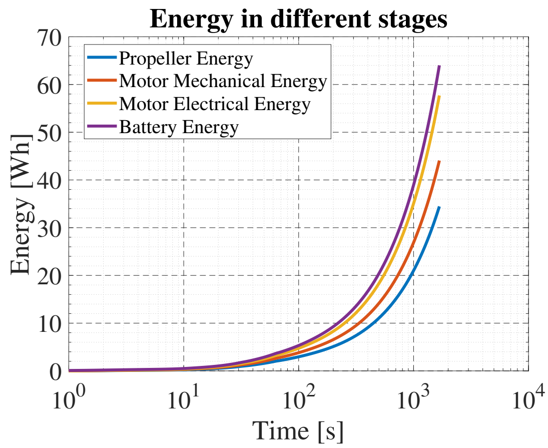

Figure 4.10: Energy consumption by the RC UAV model.

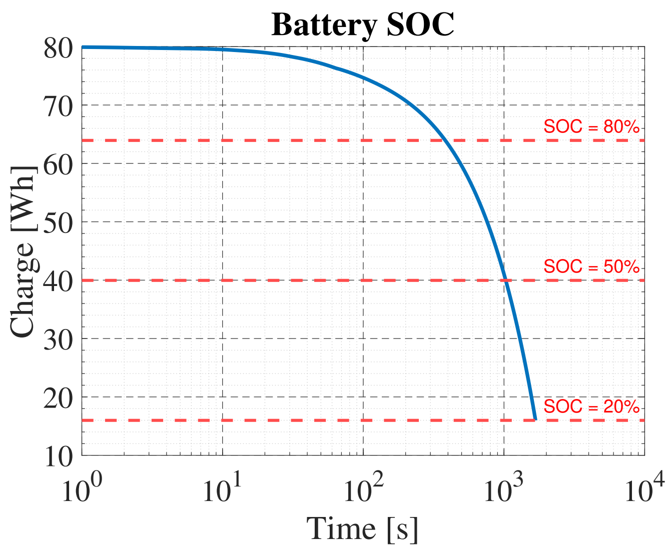

Figure 4.11: Battery SOC performed by the RC UAV model.

Regarding the previous results, it is notable that the model did not follow the speed profile (Figure 4.7) as good as it did for the trajectory profile (Figure 4.8), mainly for the first seconds of simulation and around the time it reaches the cruising speed. Both these closed-loop controllers were implemented by means of PID's, leading to some flickering and oscillations around the reference. Also, the inertia of the aircraft was not considered for the model, leading to faster movements of the aircraft - in fact, instantaneous.

At the beginning of the simulation, the aircraft's speed is above the reference because too much power is being used from the batteries. After that, during the altitude climbing, the power shows some peaks and then it stabilises to a constant value when both the altitude and speed are constant. The efficiency of the systems is evident not only in the power consumption (Figure 4.9) but also in the energy consumption (Figure 4.10).

The simulation was projected for a consumption of 80% of the total battery's energy. When this value is reached, the simulation automatically stops, as can be seen in Figure 4.11.

It was chosen to present the results in a logarithmic scale due to the long duration of the simulations, otherwise, the takeoff zone would not be visible since the aircraft stays cruising for a long interval of time.

Overall, the model's behaviour was the expected from a UAV. Hence, it can be considered validated.

4.1.2.A Speed profile impact study

To analyse the impact of the cruising speed on the aircraft's range, a few simulations were done with different speed profiles. To show these results, Table 4.5 contains the distance travelled by the model for different maximum cruising speeds.

Maximum Cruising Speed [m/s]	Distance travelled [km]	Battery Power during cruise [W]
22.68 (max)	37.9	133.5
20 $(-12\,\%)$	43.4 $(+15\,\%)$	103.4 $(-23\,\%)$
18 $(-21\,\%)$	47.1 $(+24\,\%)$	86.1 $(-36\,\%)$
17 $(-25\,\%)$	48.5 $(+28\,\%)$	79.1 $(-41\,\%)$
15 $(-34\,\%)$	49.9 $(+32\,\%)$	68.1 $(-49\,\%)$
13 $(-43\,\%)$	49.6 $(+31\,\%)$	60.3 $(-55\,\%)$
12 $(-47\,\%)$	Stall	-

Table 4.5: Distance travelled and power consumption comparison for different cruising speeds for the RC UAV Model.

From the previous table, one can see that with the decrease of the maximum cruising speed, the range of the aircraft increases, as it generates less drag which is an aerodynamic force opposed to the movement of the aircraft. Additionally, as it was expected, the power required from the batteries during the cruising altitude is also lower for lower cruising speeds.

Regarding the distance travelled, the relative reduction in the speed is approximately the same increase in the range. However, there is a point from which the distance travelled by the aircraft does not increase anymore. Also, there is a minimum speed at which the aircraft stalls, because it is not able to generate enough lift to sustain its own mass. In this case, that speed is 12 m/s.

On the other hand, the power required from the ESS during the cruising stage has a higher relative reduction compared to the relative reduction of the cruising speed. It may not be significant, but if it is guaranteed that the model will fly at lower speeds, a lighter motor could be installed, leading to a more efficient system.

Even though this model is not a passenger aircraft, it has a wide variety of applications. It can be used, for example, for fire surveillance in forests that are difficult to access by land, for security surveillance in wide areas like beaches or cities, or even to transport light items over small distances. In the scope of this thesis, this model was used as a reference calibration, before developing the more complex ones.

4.2 Case study for a two-passenger aircraft

As a second case study, a more realistic aircraft was implemented. In this case, it is a two-passenger certified electric aircraft manufactured by *Pipistrel*.

It is able to cruise with a speed of 85 knots (157 km/h) at an altitude of 4000 meters. The manufacturer ensures a range of 120 kilometers which corresponds to approximately one-hour cruising. In Figure 4.12 there is a picture of the aircraft.

Figure 4.12: Pipistrel Alpha Electro [67].

4.2.1 Data required to simulate the model

The data required to simulate the model is presented in the next tables, categorized by each subsystem in the simulation tool.

4.2.1.A Aerodynamic Model

The aerodynamic coefficients C_D and C_L were not available specifically for this model. Therefore, the ones used were extracted from [68] and correspond to a very similar aircraft. Both the speed and the trajectory profile in Figures 4.15 and 4.16 were estimated based on the information provided by the manufacturer and making sure that the acceleration was comfortable for the passengers and the climbing angle would not lead the aircraft to stall.

Table 4.6 contains the data required for the Aerodynamic Model.

Data for the Aerodynamic Model			
Name	**Symbol**	**Unit**	**Value**
Model name	-	-	*Pipistrel Alpha Electro*
Wingspan	-	m	10.5
Length	-	m	6.5
Mass	$M_{aircraft}$	kg	256
Wing Area	S	m^2	9.51
Lift Coefficient	$C_L(\alpha)$	-	Figure 4.13
Drag Coefficient	$C_D(\alpha)$	-	Figure 4.14
Speed Profile	$V(t)$	m/s	Figure 4.15
Trajectory Profile	$z(x)$	m	Figure 4.16

Table 4.6: Data required for the Aerodynamic Model of the Pipistrel. Adapted from [69].

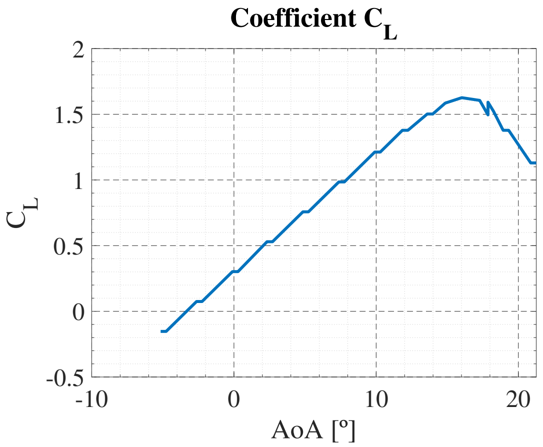

Figure 4.13: Lift coefficient C_L for the Pipistrel Model. Adapted from [68].

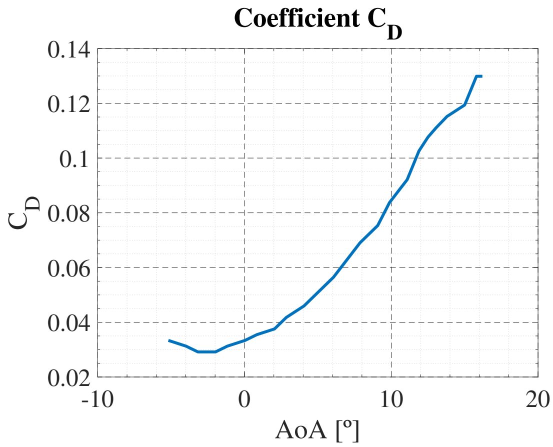

Figure 4.14: Drag coefficient C_D for the Pipistrel Model. Adapted from [68].

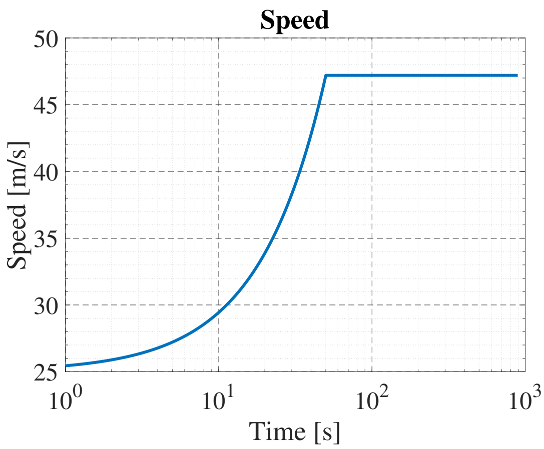

Figure 4.15: Speed profile for the Pipistrel Model.

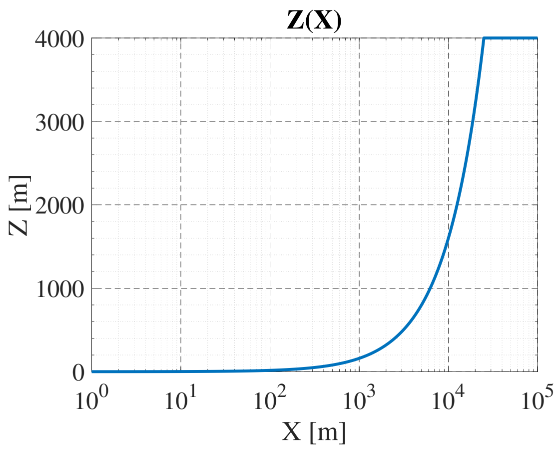

Figure 4.16: Altitude profile for the Pipistrel Model.

4.2.1.B Propeller Model

In Table 4.7, the data required to run the Propeller Model is shown.

Data for the Propeller Model			
Name	**Symbol**	**Unit**	**Value**
Model name	-	-	P-812-164-F3A
Number of Blades	-	-	3
Mass	$M_{propeller}$	kg	5
Diameter	D_p	m	1.64
Optimal Advance Ratio	J_{opt}	-	0.60
Optimal Efficiency	η_p	%	90.3

Table 4.7: Data required for the Propeller Model of the Pipistrel. Adapted from [70–72].

4.2.1.C PMSM Model

The motor used in this model is a personalized liquid-cooled motor built by *EMRAX* and *Emsiso*. Its technical data is not publicly available so, based on a similar public model, some adjustments were made so that the model could match the aircraft requirements. These modifications were mainly the change of the number of pole pairs and the corresponding synchronous speed. Table 4.8 contains the data required to run the PMSM Model.

Data for the PMSM Model			
Name	**Symbol**	**Unit**	**Value**
Model name	-	-	Pipistrel E-811-268MVLC
Motor type	-	-	Axial Flux PMSM
Pole Pairs	n_{pp}	-	4
Mass	M_{motor}	kg	22.7
Diameter	-	mm	268
Length	-	mm	91
Nominal Power	P_N	kW	46.1
Nominal Voltage	U_N	Vrms	169
Nominal Frequency	f_N	Hz	146.7
Nominal Torque	T_N	Nm	200
Nominal Speed	N_N	rpm	2200
Nominal Current	I_N	A	160
Nominal Efficiency	η_N	%	96.9
Direct and Quadrature Inductance	L_d, L_q	μH	39
Stator Resistance	R_s	Ω	0.007
Permanent Magnet Flux	λ_{PM}	Wb	0.1473
No-Load Power	P^0_{motor}	kW	1 @ 2200 rpm

Table 4.8: Data required for the PMSM Model of the Pipistrel. Adapted from [73, 74].

4.2.1.D Battery Model

In Table 4.9, the data required for the Li-ion Battery Model is detailed.

Data for the Li-ion Battery Model			
Name	**Symbol**	**Unit**	**Value**
Battery Type	-	-	Li-NMC
Mass	M_{bat}	kg	2×72
Length	-	mm	546
Width	-	mm	265
Height	-	mm	375
Nominal Voltage	U_N	V	345
Storage Capacity	E_{full}	Ah	2×30
Electronic Equipment Efficiency	$\eta_{e.e}$	$\%$	95
Battery Efficiency	η_{bat}	$\%$	95

Table 4.9: Data required for the Battery Model of the Pipistrel. Adapted from [69, 75].

4.2.2 Simulation Results

With the data specified in Section 4.2.1, the model was simulated and the results are shown ahead. In Figure 4.17 the aircraft's speed with the respective reference is presented. Figure 4.18 shows the trajectory followed by the aircraft, as well as its reference. In Figures 4.19 and 4.20 the power and energy consumption for each system individually can be seen. With respect to the last subsystem, Figure 4.21 contains the Battery's SOC.

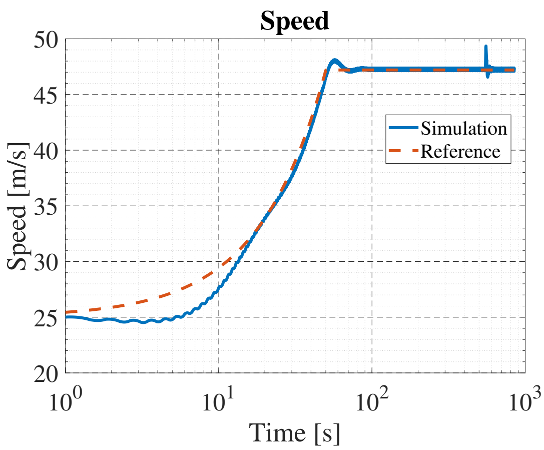

Figure 4.17: Speed performed by the Pipistrel model.

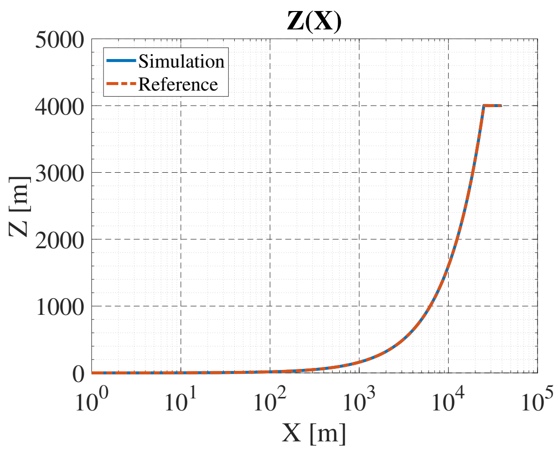

Figure 4.18: Trajectory followed by the Pipistrel model.

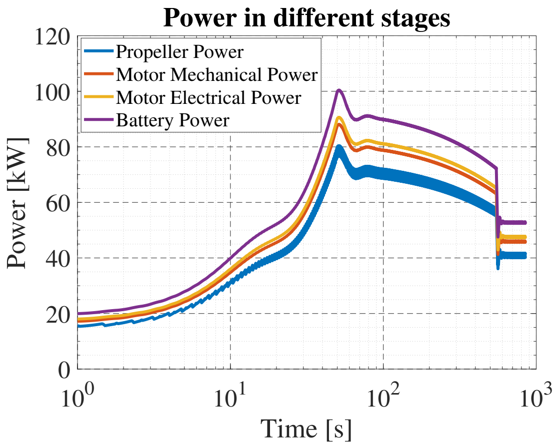

Figure 4.19: Power consumption by the Pipistrel model.

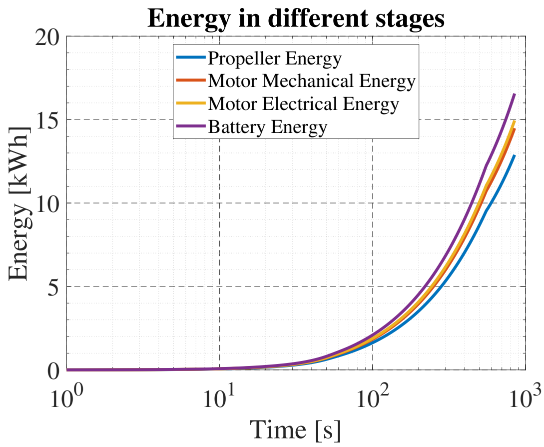

Figure 4.20: Energy consumption by the Pipistrel model.

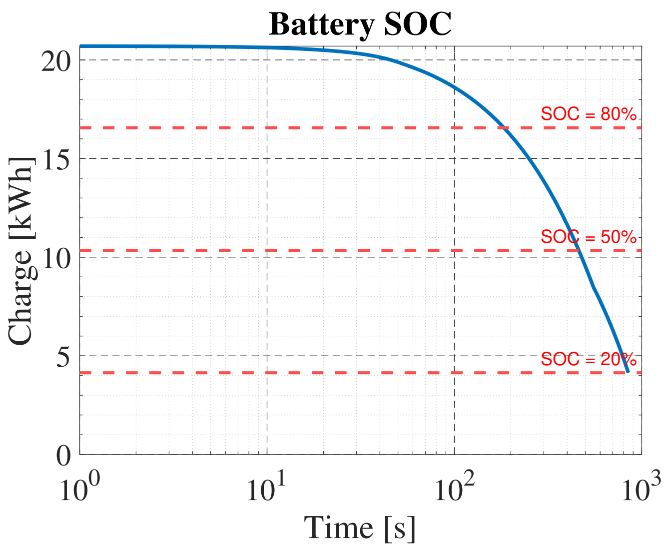

Figure 4.21: Battery SOC performed by the Pipistrel model.

Overall, this model presents more stable and steady results than the previous one, but this is verified mainly in the speed profile (Figure 4.17), where it presents fewer spikes and a lower error during the first seconds of the simulation. This can be caused by a better tuning of the PID controllers.

As for the altitude in Figure 4.18, this aircraft requires a higher distance to reach the cruising altitude, as it is higher than the one for the RC UAV.

Regarding the power consumption for the four different systems, the curves are close to each other, meaning that the systems have high efficiency. By analysing the shape of the curve, while the aircraft is climbing and increasing the speed at the same time, the power required keeps increasing. First, the aircraft reaches the cruising speed during its climb conditions, so the power required suffers a slight decrease, but the highest reduction to a constant steady value happens when the model reaches the cruising altitude.

During the climbing stage, it is visible a peak of almost twice the nominal power. Afterwards, when the aircraft reaches cruising altitude, the motor's consumption power is very close to the nominal one. In fact, the climb rate and the speed profile could be less steeply so that the motor's peak power would be lower. This is dangerous for the motor and actually, it may not be able to deliver that amount of power. Specifically, a typical PMSM can withstand up to 150% of the rated torque during a short time period, so 200% is still far from the motor's safe conditions [76].

Similarly to the previous model, the simulation was projected for a consumption of 80% of the total battery's energy. When this value is reached, the simulation automatically stops, as can be seen in Figure 4.21.

4.2.2.A Speed profile impact study

To analyse the impact of the cruising speed on the aircraft's range, a few simulations were done with different speed profiles. Hence, Table 4.10 contains the distance travelled by the model for different maximum cruising speeds.

Maximum Cruising Speed [m/s]	Distance travelled [km]	Battery Power during cruise [kW]
47.2 (max)	39.0	52.8
$42\ (-11\,\%)$	$48.3\ (+24\,\%)$	$38.5\ (-27\,\%)$
$37\ (-22\,\%)$	$62.1\ (+59\,\%)$	$18.6\ (-65\,\%)$
$30\ (-36\,\%)$	$88.4\ (+126\,\%)$	$12.2\ (-77\,\%)$
$27\ (-43\,\%)$	$104.6\ (+168\,\%)$	$10.1\ (-81\,\%)$
$22\ (-53\,\%)$	$124.5\ (+219\,\%)$	$8.3\ (-84\,\%)$
$21\ (-56\,\%)$	Stall	-

Table 4.10: Distance travelled and power consumption comparison for different cruising speeds for the Pipistrel Model.

As already seen in the previous experiment, with the decrease of the maximum cruising speed, the aircraft's range increases and the power required from the battery decreases. However, the results shown for this model demonstrate even a higher impact than for the previous one.

In Figure 4.19, it was seen that the motor's peak power was considerably above the rated one and the cruising one was approximately the rated. But with these results, it can be confirmed that if the aircraft does not travel at its maximum cruising speed, the power demanded from the motor is lower, thus allowing it to work at a more efficient point.

With just a decrease of 11% in the cruising speed, the aircraft's range increases by 24%, and the power required from the batteries reduce by 27%. Yet, if the speed continues to reduce, the range of the aircraft can increase more than twice the original range. Obviously, by choosing a lower cruising speed, the travel time increases, so it should be planned in advance depending on each flight situation.

Based on this study, the aircraft has to cruise with a speed of 22 m/s in order to have the range that the manufacturer guarantees, which is approximately half of the standard cruising speed. Of course, this deviation may come from the drag and lift coefficients considered here, due to the lack of information from the *Pipistrel* manufacturer.

4.2.2.B Cruising altitude impact study

In a second study, the cruising altitude was changed in order to analyse the impact on the aircraft's range and the power required from the battery during the cruising altitude and speed. Four simulations were done with a constant cruising speed of 30 m/s and the results are shown in Table 4.11.

Maximum Cruising Altitude [m]	**Distance travelled [km]**	**Battery Power during cruise [kW]**	**Energy consumption during takeoff [kWh]**	**Energy consumption during cruise [kWh]**
4000 (max)	88.4	12.2	9.1	7.5
3000 ($-25\,\%$)	97.2 ($+10\,\%$)	12.8 ($+5\,\%$)	7.6 ($-16\,\%$)	9.0 ($+20\,\%$)
2000 ($-50\,\%$)	115.2 ($+30\,\%$)	12.8 ($+5\,\%$)	5.6 ($-38\,\%$)	11.0 ($+47\,\%$)
1000 ($-75\,\%$)	122.6 ($+37\,\%$)	13.8 ($+13\,\%$)	4.5 ($-51\,\%$)	12.1 ($+61\,\%$)

Table 4.11: Distance travelled and power consumption comparison for different cruising altitudes for the Pipistrel Model.

As it was expected, by reducing the cruising altitude, the aircraft increases its range, as the total energy required to climb is lower, therefore increasing the distance that it can travel while cruising, with the same percentage of the battery used. As the aircraft travels a higher distance, the energy consumption during this stage will be higher. But it will increase with a higher relation than the range, as this is not the optimal altitude for the aircraft to cruise, meaning that the aircraft will spend more energy per kilometer travelled, for lower altitudes.

Regarding the power consumed from the battery during cruising, it shows a slight increase with the decrease of the cruising altitude. At lower altitudes, the air density is higher, due to the higher concentration of particles. As it was demonstrated in Section 3.1.3, the Drag magnitude is directly proportional to the air density (Equations (3.10) and (3.11)). Hence, for lower altitudes, it is required more power to keep the same velocities, when the aircraft is cruising.

4.2.2.C Battery types impact study

The final study for this model covers the impact of choosing the right battery type for the aircraft. On one side, having a high mass of batteries, allows the aircraft to spend a higher amount of energy, thus increasing its range. But, the drawback is that by increasing the aircraft's mass, it will require a higher lift to compensate for the extra mass, and, for the same speed, means that it will need a higher angle of attack and thrust are required from the propellers during the cruise, becoming less efficient with a higher energy consumption per kilometer. Therefore, by choosing a battery type with a higher energy density, there will be more energy available with a lower mass contribution.

For this study, the energy to be available in the batteries is fixed as the same as the original aircraft (20.7 kWh). Different batteries will be tested, with different energy densities, leading to a different battery mass.

In Table 4.12, the different simulations can be compared, where it is shown the type of battery used, its respective mass, the distance travelled by the aircraft and the battery power during the cruising stage. The results shown are for a cruising speed of 30 m/s and a cruising altitude of 4000 meters.

Battery Type	Energy Density [Wh/kg]	Battery Mass [kg]	Distance travelled [km]	Battery Power during cruise [kW]
Li-NMC (manufacturer)	143.75	144	88.4	12.2
Lead-Acid	$40\ (-72\,\%)$	$517.5\ (+259\,\%)$	$52.2\ (-41\,\%)$	$20.5\ (+68\,\%)$
NiCd	$50\ (-65\,\%)$	$414\ (+188\,\%)$	$60.1\ (-32\,\%)$	$17.7\ (+45\,\%)$
LiPo	$100\ (-30\,\%)$	$207\ (+44\,\%)$	$81.5\ (-8\,\%)$	$12.9\ (+6\,\%)$
$LiFePO_4$	$125\ (-13\,\%)$	$165.6\ (+15\,\%)$	$86.0\ (-3\,\%)$	$12.4\ (+2\,\%)$
$LiMnPO_4$	$150\ (+4\,\%)$	$138\ (-4\,\%)$	$89.0\ (+1\,\%)$	$12.1\ (-1\,\%)$
Li-NMC (better)	$200\ (+39\,\%)$	$103.5\ (-28\,\%)$	$92.6\ (+5\,\%)$	$11.6\ (-5\,\%)$

Table 4.12: Distance travelled, power and energy consumption comparison for different battery technologies for the Pipistrel Model.

Clearly, the battery design for electrical aircraft is a very critical challenge, as it contributes with a very high share to the total aircraft's mass.

On one hand, if the set of batteries chosen is the one with the lowest energy density, the battery mass increase to more than threefold (259%) and the range is reduced to 41% of the original range. Also, the motor may have to be redesigned, because the power required from the batteries during the cruise is 68% higher.

On the other hand, by choosing the best technology, with a higher energy density, there is a decrease of almost 30% in the mass, but only a range 5% higher. The impact on the battery power is also not very significant, as it is only 5% lower than the original motor.

So, to sum up, designing the battery system is very important and challenging, because the impact of worse battery technology may be higher than the benefit of a better technology with the same mass variation. There is a point from which the extra investment is not worth it because the reduction in mass will not increase the range in the same proportion.

4.3 Case study for a Commercial Aircraft

As a final model, a fuel-powered aircraft will be studied. It is widely used in Portugal for inter-island connections and the goal for this stage is to study how this aircraft could be converted into an AEA.

The *Bombardier Q400 Nextgen* has a capacity for 70 passengers with two fuel-powered engines that provide a range of 2500 kilometers. It can cruise with speeds up to 360 knots (667 km/h) and at an altitude of 8200 meters. In Figure 4.22, a picture of this aircraft can be seen.

With this model, the goal is to study the conversion of a regular fuel-powered aircraft to an electric one. The combustion motors are going to be replaced by electric ones and the fuel storage system by an electric ESS.

Figure 4.22: Bombardier Q400 Nextgen [77].

4.3.1 Data required to simulate the model

The data required to simulate the model is presented in the next tables, categorized by each subsystem in the simulation tool.

4.3.1.A Aerodynamic Model

Similarly as it happened for the previous model, the aerodynamic coefficients C_D and C_L were not available specifically for this aircraft. Therefore, the ones used were extracted from [78] and correspond to a very similar aircraft. Both the speed and the trajectory profile in Figures 4.25 and 4.26 were estimated based on the information provided by the manufacturer and making sure that the acceleration was comfortable for the passengers and the climbing angle would not lead the aircraft to stall.

Table 4.13 contains the data required for the Aerodynamic Model.

Data for the Aerodynamic Model			
Name	**Symbol**	**Unit**	**Value**
Model name	-	-	*Bombardier Q400*
Wingspan	-	m	28.4
Length	-	m	32.8
Mass	$M_{aircraft}$	kg	25000
Wing Area	S	m^2	63.1
Lift Coefficient	$C_L(\alpha)$	-	Figure 4.23
Drag Coefficient	$C_D(\alpha)$	-	Figure 4.24
Speed Profile	$V(t)$	m/s	Figure 4.25
Trajectory Profile	$z(x)$	m	Figure 4.26

Table 4.13: Data required for the Aerodynamic Model of the Commercial Aircraft. Adapted from [79].

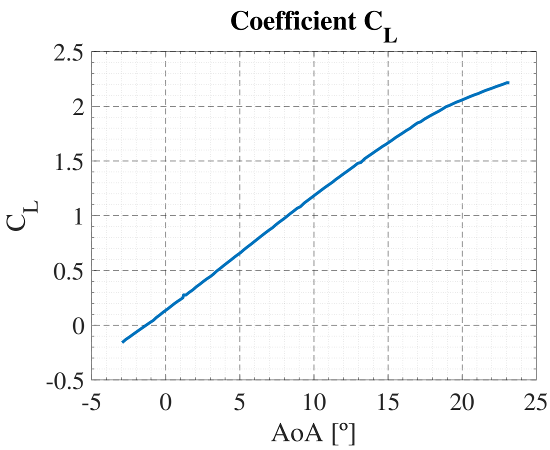

Figure 4.23: Lift coefficient C_L for the Commercial Aircraft Model. Adapted from [78].

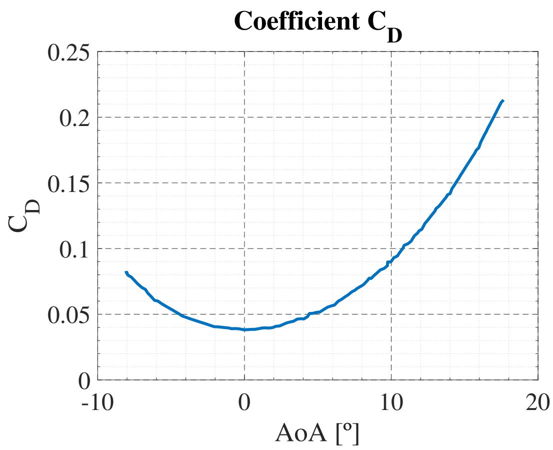

Figure 4.24: Drag coefficient C_D for the Commercial Aircraft Model. Adapted from [78]

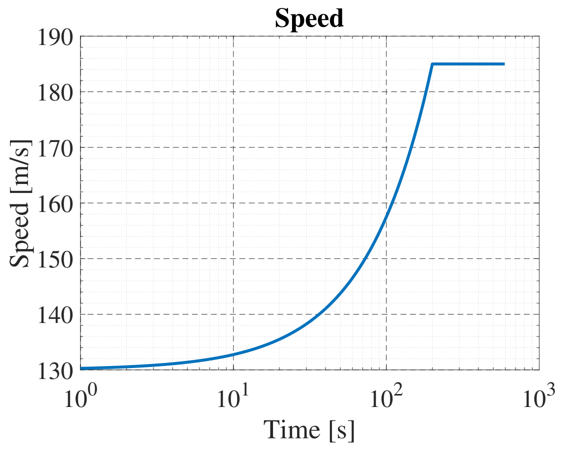

Figure 4.25: Speed profile for the Commercial Aircraft Model.

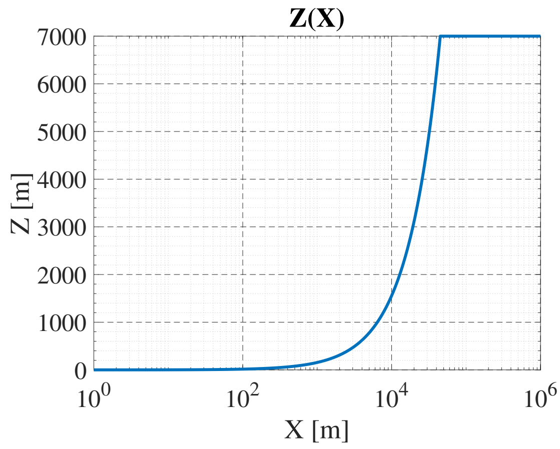

Figure 4.26: Altitude profile for the Commercial Aircraft Model.

4.3.1.B Propeller Model

As it will be seen ahead, there are going to be required 4 motors for this aircraft. So, in Table 4.14, the data required to run the Propeller Model is shown, considering the 4 propellers.

Data for the Propeller Model			
Name	**Symbol**	**Unit**	**Value**
Model name	-	-	Dowty R408
Number of Blades	-	-	6
Mass	$M_{propeller}$	kg	4×252
Diameter	D_p	m	4.1
Optimal Advance Ratio	J_{opt}	-	2.13
Optimal Efficiency	η_p	%	0.87

Table 4.14: Data required for the Propeller Model of the Commercial Aircraft. Adapted from [80, 81].

4.3.1.C PMSM Model

The original aircraft only has 2 motors, however, with the additional mass of the batteries, they did not provide enough thrust to generate lift to the aircraft. Therefore, 2 motors were added to the model, adding up to 4. Table 4.15 contains the data required to run the PMSM Model. To be noted that this is a PMSM with conventional materials, so its mass is very high. Later on, a high-temperature superconductor motor will be considered.

Data for the PMSM Model			
Name	**Symbol**	**Unit**	**Value**
Motor type	-	-	PMSM
Pole Pairs	n_{pp}	-	2
Mass	M_{motor}	kg	4×5056.8
Diameter	-	mm	385
Length	-	mm	1000
Nominal Power	P_N	MW	5
Nominal Voltage	U_N	Vrms	590.3
Nominal Frequency	f_N	Hz	50
Nominal Torque	T_N	kNm	32
Nominal Speed	N_N	rpm	1500
Nominal Current	I_N	A	6400
Nominal Efficiency	η_N	%	99
Direct and Quadrature Inductance	L_d, L_q	μH	71.3
Stator Resistance	R_s	$m\Omega$	0.3125
Permanent Magnet Flux	λ_{PM}	Wb	1.18
Iron Losses	$P_{iron,loss}$	W	9065
Mechanical Losses	$P_{mec,loss}$	W	9065

Table 4.15: Data required for the PMSM Model of the Commercial Aircraft. Adapted from [82]

4.3.1.D Battery Model

As the original version of this aircraft is not an electric-powered one, the battery design is generic and therefore, several simulations on the batteries' mass will be shown ahead. Beforehand, a battery type is chosen with a very high energy density.

In Table 4.16, the data required for the Li-ion Battery Model is detailed.

Data for the Li-ion Battery Model			
Name	**Symbol**	**Unit**	**Value**
Battery Type	-	-	Li-NMC
Energy Density	ρ_{bat}	Wh/kg	200
Electronic Equipment Efficiency	$\eta_{e.e}$	$\%$	95
Battery Efficiency	η_{bat}	$\%$	95

Table 4.16: Data required for the Battery Model of the Commercial Aircraft. Adapted from [35].

4.3.2 Simulation Results

With the data specified in Section 4.3.1, the model was simulated and the results are shown ahead for different studies.

Firstly, the impact of the battery mass is studied, with a fixed energy density. Secondly, the maximum cruising speed is changed in order to analyse its effect on the aircraft's range. Then, a case study considering superconducting motors is considered for this model and, last but not least, a fuel cell is simulated and its results are analysed.

4.3.2.A Battery mass impact study

As the first study for this model, the battery mass was changed with the energy density fixed. In Table 4.17, for each simulation, the energy available in the batteries, the distance travelled and the motor's peaks and average powers can be seen.

Battery Mass [kg]	Energy Available [MWh]	Distance travelled [km]	Motor peak take-off power [MW]	Motor average cruise power [MW]
10000	2	39.8	23.0	-
15000	3	70.0	24.3	12.0
20000	4	102.3	25.9	12.3
25000	5	132.1	27.2	12.7
30000	6	159.4	28.7	13.1
35000	7	185.5	30.2	13.2
40000 (max)	8	207.1	31.9	15.0

Table 4.17: Distance travelled and power consumption comparison for different battery mass for the Commercial Aircraft Model.

According to [76], a PMSM can run between 35% and 50% above its rated power for a few minutes without damaging it. Therefore, based on the previous results from Table 4.17, the maximum battery mass that the corresponding motor's peak power below this limit is for a battery mass of 25 tons with 5 MWh of energy available.

For this mass, in Figure 4.27 the aircraft's speed with the respective reference is presented. Figure 4.28 shows the trajectory followed by the aircraft, as well as its reference. And in Figures 4.29 and 4.30 the power and energy consumption for each system individually can be seen.

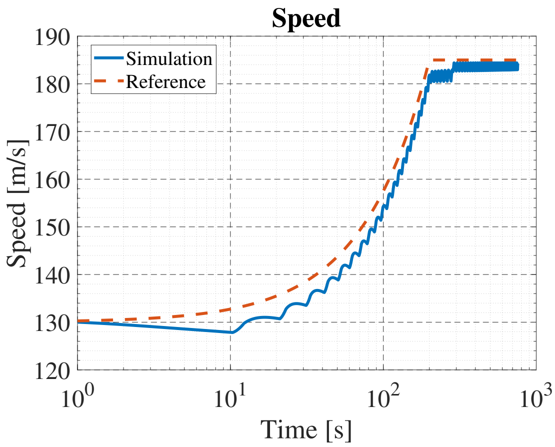

Figure 4.27: Speed performed by the Commercial Aircraft model.

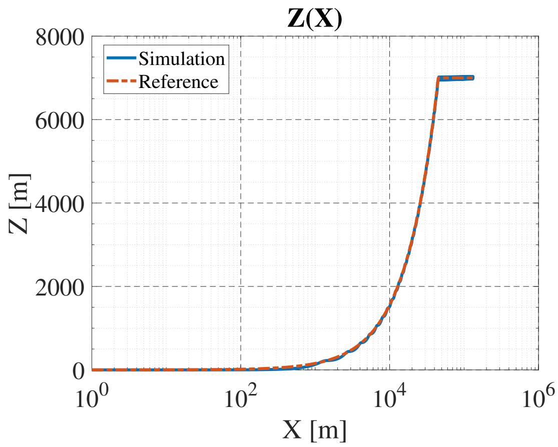

Figure 4.28: Trajectory followed by the Commercial Aircraft model.

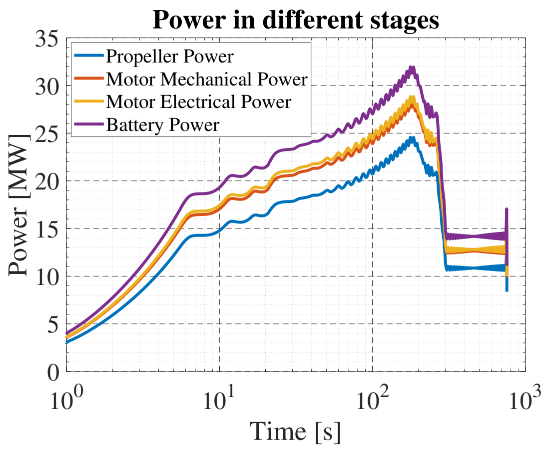

Figure 4.29: Power consumption by the Commercial Aircraft model.

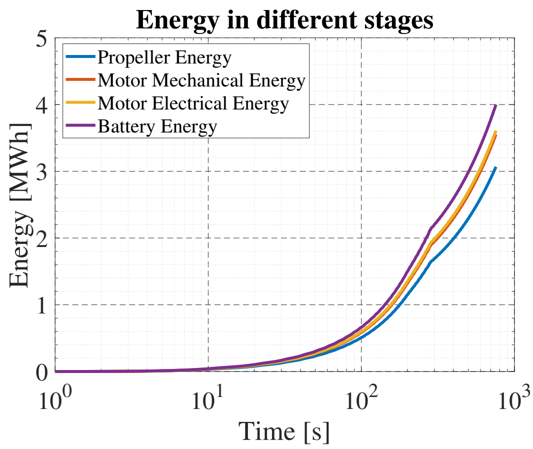

Figure 4.30: Energy consumption by the Commercial Aircraft model.

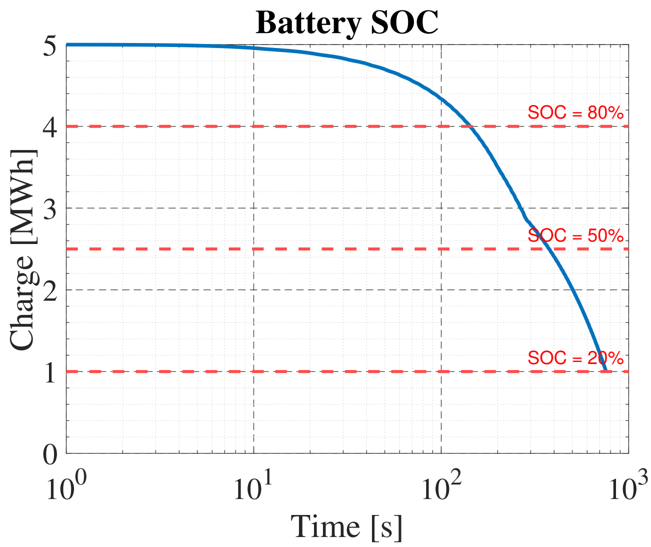

Figure 4.31: Battery SOC performed by the Commercial Aircraft model.

Regarding the results of this model, both the speed (Figure 4.27) and the trajectory profiles (Figure 4.28) are followed with a small error. Even though there is some noise and flickering, its impact is low, meaning that the PID was correctly tuned. Also, regarding the trajectory, for this battery mass, knowing that the fuel-powered aircraft can fly up to 2500 kilometers, the electrified version only has a range of 132.1 kilometers, which corresponds to a decrease of about 95%. The new range can limit the current trajectories flown by this aircraft. Note that this simulation was performed for the maximum cruising speed that the aircraft can fly, but ahead this impact will also be studied.

Regarding the power in Figure 4.29, one can see that the power required increases until the aircraft reaches its cruising altitude and cruising speed. Relating it with the energy consumed in Figure 4.30 and the battery SOC in Figure 4.31, it corresponds to the same time instant where the slope of the curve decreases, as the power also decreases and the energy is the power integral.

4.3.2.B Speed profile impact study

As a second study, the cruising speed impact will be studied considering a mass of 25 tons for the batteries. For this, in Table 4.18, the distance travelled by the aircraft is shown, as well as the battery's power during the cruise for different cruising speeds.

Maximum Cruising Speed [m/s]	Distance travelled [km]	Battery Power during cruise [MW]
185 (max)	132.1	14.2
180 $(-3\,\%)$	135.7 $(+3\,\%)$	13.4 $(-6\,\%)$
170 $(-8\,\%)$	144.5 $(+9\,\%)$	12.1 $(-15\,\%)$
160 $(-14\,\%)$	155.0 $(+17\,\%)$	11.3 $(-20\,\%)$
150 $(-19\,\%)$	166.2 $(+26\,\%)$	10.7 $(-25\,\%)$
140 $(-24\,\%)$	177.2 $(+34\,\%)$	9.9 $(-30\,\%)$
130 $(-30\,\%)$	188.4 $(+43\,\%)$	9.2 $(-35\,\%)$

Table 4.18: Distance travelled and power consumption comparison for different cruising speeds for the Commercial Aircraft Model.

As it was expected, when the cruising speed decreases, the same energy provides the aircraft with a higher range. From the results in Table 4.18, the relation is approximately linear. The relative decrease in the cruising speed leads to a similar relative increase in the range and also a similar decrease in the battery power required during the cruise.

Even the maximum range obtained from these simulations is not comparable with the fuel-powered aircraft. But, by reducing the cruising speed by 30%, the range is 43% higher than the one for the standard cruising speed. Of course, the drawback of reducing the speed is that the time required for a trip increases, and passengers may not be open to that possibility.

Another result to look through is the battery power during the cruise. By reducing the speed, the power required during the cruising stage decreases and this can have a significant impact on the model. First, by reducing the power, the rotational speed of the motors decreases, generating less noise, thus providing a more comfortable flight for the passengers. But, maybe the most important conclusion is that with a lower cruising speed, the motors may be oversized and therefore, the number of motors or the nominal power can be reduced. This not only has a direct impact on the model's mass (increasing, even more, the range), but also on the price.

For this specific example, if is it assured a cruising speed of 130 m/s, the number of motors could be reduced to 2 instead of 4 as they would provide a nominal power of 10 MW, that is enough for this speed. As each motor weights approximately 5 tons, if this mass was replaced by batteries, by adding 10 tons of batteries, the aircraft would have an additional range of approximately 40 kilometers (check Table 4.17).

For this aircraft, a study on changing the cruising altitude would not be useful since passenger aircraft fly at high altitudes, generally above 30000 feet (9144 meters). With fewer particles present in the air less drag is generated leading to higher overall flight efficiencies.

4.3.2.C Superconducting motor study

As seen with the previous results, the main challenge of electric aircraft is the mass of its components. One possible solution to be implemented in future electric aircraft might be superconducting motors, as they have a higher power density, therefore having the same power available with less mass.

For this passenger model, the motor implemented uses High Temperature Superconductors (HTS) which is seen today as a potential technology to increase the power density of electric motors [83].

Due to the high complexity of this motor, its implementation was only considering the efficiency. Since this is only a preliminary case study, the phenomena of superconductivity are not considered here. The power and energy required from the motor are calculated by dividing the power and energy required by the propeller by the motor efficiency, respectively. In Table 4.19, the details of this Superconducting motor can be seen.

Data for the Superconducting HTS-PMSM			
Name	**Symbol**	**Unit**	**Value**
Motor type	-	-	HTS-PMSM
Pole Pairs	n_{pp}	-	4
Mass of the motor	M_{motor}	kg	2×422.0
Mass of the cryostat	$M_{cryostat}$	kg	1200
Diameter	-	mm	295
Length	-	mm	645
Nominal Power	P_N	MW	10
Nominal Voltage	U_N	kVrms	2.12
Nominal Torque	T_N	kNm	13.9
Nominal Speed	N_N	rpm	6870
Nominal Current	I_N	A	8451
Nominal Efficiency	η_N	%	98.4

Table 4.19: Data required for the Superconducting PMSM Model of the Commercial Aircraft. Adapted from [83, 84]

In Table 4.20 the results using the superconducting motor are shown. For comparison, in the last two columns, the results with the previous PMSM are available. The percentages presented correspond to the relative change with respect to the respective cruising speed with the regular PMSM.

	Superconducting Motor		Regular PMSM	
Maximum Cruising Speed [m/s]	**Distance travelled [km]**	**Battery Power during cruise [MW]**	**Distance travelled [km]**	**Battery Power during cruise [MW]**
185 (max)	169.6 (+28 %)	12.1 (−15 %)	132.1	14.2
180	173.9 (+28 %)	11.4 (−15 %)	135.7	13.4
170	185.7 (+29 %)	10.3 (−15 %)	144.5	12.1
160	197.2 (+27 %)	9.2 (−19 %)	155.0	11.3
150	210.3 (+27 %)	8.0 (−25 %)	166.2	10.7
140	224.6 (+27 %)	7.3 (−26 %)	177.2	9.9
130	236.3 (+25 %)	6.9 (−25 %)	188.4	9.2

Table 4.20: Distance travelled and power consumption comparison for different cruising speeds for the Commercial Aircraft Model with superconducting motors.

The implementation of this superconducting motor highly reduces the total aircraft mass. For the same nominal power, the regular PMSM has a total mass of approximately 20 tons, whereas the superconducting one has a total mass of 2 tons, including the cryostat, which is about 10% of the first one. Plus, given the higher power density, only 2 motors are required, instead of 4.

The results in Table 4.20 show an increase in the aircraft's range and a decrease in the power required from the battery. With this superconducting motor, the aircraft can travel almost 30% longer with about 20% less power required from the batteries.

The drawback of this implementation is that this type of motors are not yet publicly available. They are still under research and testing, as very expensive materials are required to build them.

4.3.2.D Fuel cell study

As in the last study, a preliminary case study using fuel cells is considered. As seen in Section 2.2.2, unlike batteries, they have lower efficiency, but on the other side higher energy and power densities. For this study, a specific model was not chosen, thus a range of energy densities will be tested.

In Table 4.21 the details of the fuel cell model are available.

Data for the Fuel-cell Model			
Name	**Symbol**	**Unit**	**Value**
Mass	M_{fuel_cell}	kg	25000
Energy Densities	$\rho_{fuel-cell}$	Wh/kg	500 − 1000
Electronic Equipment Efficiency	$\eta_{e.e}$	%	95
Fuel cell Efficiency	η_{fuel_cell}	%	55

Table 4.21: Data required for the Fuel cell Model of the Commercial Aircraft. Adapted from [35, 41].

There are advantages of using fuel cells with superconducting motors since the hydrogen of the fuel cell can be used for cooling the superconducting parts of the motor [25]. Therefore, for this simulation, the fuel cells were implemented with the superconducting motor.

For this simulation, the mass of the fuel cells was fixed to be the same as with the previous batteries for this aircraft which is 25 tons. But by testing different energy densities, the energy available changes. The results are shown in Table 4.22 and correspond to the standard cruising speed of 185 m/s.

Fuel cell Energy Density [Wh/kg]	Energy Available [MWh]	Distance travelled [km]
500	12.5	267.1
600 (+20 %)	15.0 (+20 %)	330.1 (+24 %)
700 (+40 %)	17.5 (+40 %)	393.1 (+47 %)
800 (+60 %)	20.0 (+60 %)	456.1 (+71 %)
900 (+80 %)	22.5 (+80 %)	519.1 (+94 %)
1000 (+100 %)	25.0 (+100 %)	582.1 (+118 %)

Table 4.22: Distance travelled for different Fuel cell energy densities for the Commercial Aircraft Model with superconducting motors.

By analysing the previous results, it is seen, as expected, that when using fuel cells with higher energy density the range increases. As the mass does not change, the only variable changing is the energy available. Therefore, by increasing the energy density, the energy available increases, leading to a higher range. For this study, the power is not shown as it was constant for all the simulations, due to the equal mass between the simulations.

An important remark to be made is that the distance travelled by the aircraft increases in a higher proportion than the relative increase in the energy available in fuel cells. This is a prosperous result, as it shows the high potential of using this technology. Despite the low efficiency of the fuel cells, the very high energy density provides the aircraft with a higher range than the battery-equipped aircraft.

In addition, for this study, the fuel cells were combined with the superconducting motor. Not only do these technologies provide the aircraft with lighter systems when compared to batteries and the PMSM, respectively, but can also cooperate together by using the hydrogen of the fuel cell as a cooling system for the superconducting motor.

Overall, this model presented very satisfactory results. With a regular PMSM implemented, it can travel between 132 and 188 kilometers, depending on the cruising speed, which is only about 6% of the range of the original fuel-powered aircraft. When superconducting motors are installed with batteries, the aircraft's range is between 170 and 236 kilometers, depending on the cruising speed, however, these motors are not yet available in the market. Furthermore, when superconducting motors are combined with fuel cells, the best results are achieved, where the aircraft's range can increase up to 585 kilometers for the standard cruising speed. But, like superconducting motors, it is challenging to build high energy density fuel cells, and this might be a long-term solution. All in all, a short-term solution could be implemented with the usage of regular PMSM and batteries.

5

Conclusion and Future Work

Contents

5.1 Conclusions

In this thesis, it was possible to do a comparative study to analyse the transition of the aeronautical sector to an electrified one. For this purpose, a simulation environment was built to allow modelling an electric aircraft that already exist and to study the conversion of a fuel-power aircraft to an electric one. Furthermore, different technologies were used when it concerns electric motors and ESS.

For this, the simulation model was divided into 4 main blocks - Aircraft Aerodynamics, Propeller, Electric Motor and ESS - and the implementation of those was detailed in Chapter 3. Since the main goal was to estimate the energy and power consumption, a few simplifications were considered. In the aerodynamic model, the inertia of the aircraft was neglected as well as the takeoff acceleration since the simulation starts at the point that the aircraft leaves the ground. Within the propeller, it was considered an operation under the optimal efficiency and advance ratio, whereas, in reality, this may not happen, leading to lower efficiencies. In what concerns the electric motor, the models were implemented in detail, except the superconducting one, where due to the high complexity of this technology, only its efficiency and power density were considered. For the ESS, the model was very simplified, as only two efficiencies were considered - one for the ESS itself and another for auxiliary electronic equipment.

In Chapter 4, the data required for the implementation of the models were detailed alongside the respective results for each model. Regarding the first model, the RC UAV, its main goal was to verify and validate the aerodynamic model and it was considered as achieved. In addition, it was identified that the PID controllers were not correctly tuned, as some noise and flickering was present in the velocity and position. Some possible applications for this aircraft are surveillance of remote areas to detect fires or for medical emergency, for example.

As for the second case-study, the Pipistrel Alpha Electro is a two-passenger aircraft that already exists and is able to perform some low-range trips without relying on fuel. The implementation of this model carried the uncertainty of the drag and lift coefficients as well as the motor's model, since these data was not publicly available. Therefore, based on the simulations performed, the model can only fly the range provided by the manufacturer, when cruising at half of the maximum cruising speed. It was also noted that a change on the cruising altitude have an significant impact on the range as it can increase up to 37% and even more if this reduction is conjugated with a reduction on the cruising speed. Yet, this can jeopardize the flight security, so it has to be planned accordingly with the atmospheric conditions and safety standards. Different battery technologies was also studied and the conclusion is that it is a fundamental choice as a lower energy density on the battery can sharply reduce the aircraft's range and increase the power required from the motor.

The third and last case-study was a fuel-powered aircraft and the goal was to analyze its conversion into an AEA. This is a passenger aircraft with a capacity for 70 people, so there is a very high interest in electrifying this spectrum of aircraft as it can be an in intermediate step before larger aircraft. In the first implementation, batteries and a PMSM were used, this model presented a significantly lower range than the original fuel-powered version. But, when compared to the Pipistrel, it comes with the advantage of a higher range and also a higher passenger capacity. When the superconducting motor is installed, the motor's mass reduces to about 10%, when comparing with the PMSM. With a lower mass, the range increases about 25% and the number of motors required may reduce, as less power is required from the motor. When the superconducting motor is used with fuel cells, the distance travelled by the aircraft increases due to the high energy density of the fuel cells. Different energy densities were tested, and it was seen that with best technologies, the range can double. However, these technologies are still under research and development, so this might only be a long-term solution.

Another important challenge with AEA regarding its batteries has to do with the charging time. It shall be taken into account that, unlike conventional aircraft that fill up their tanks within a few minutes, an AEA would require maybe a few hours, depending on the charging power. This may turn the investment less interesting for airline companies, as that aircraft would perform less flights, thus not recovering back the initial investment. One possible solution for small AEA would be the installation of removable batteries, but this can be more challenging for future commercial AEA, as the batteries are distributed along the aircraft body.

5.2 Future Work

In the aerodynamic model of this thesis, the inertia of the aircraft was not considered for simplification of the dynamic equations of motion. However, this simplification does not match with the reality. Therefore, for a more accurate simulation, it should be considered. Still in the aerodynamic model, the energy and power consumed during the motor's start-up, taxi and takeoff should also be simulated for a more complete energy study.

Regarding the propeller, a more accurate implementation would include a closed-loop control system for the advance ratio and efficiency, as this system does not always operate at its maximum efficiency point.

In the ESS, the voltage and current should also be controlled, and a dependency on the temperature should be considered for the efficiency.

A more complete and detailed analysis must also include an economic viability study to complement the energy study one, as some components can be very expensive and its cost-benefit should be appraised.

Bibliography

[1] E. European Environment Agency, European Union Aviation Safety Agency, *European Aviation Environmental Report 2019*, January 2019. [Online]. Available: https://www.eurocontrol.int/publication/european-aviation-environmental-report-2019

[2] G. G. Fleming and I. de Lépinay, *Environmental Trends in Aviation to 2050*, International Civil Aviation Organization, 2019. [Online]. Available: https://www.icao.int/environmental-protection/Documents/EnvironmentalReports/2019/ENVReport2019_pg17-23.pdf

[3] J. Larsson, A. Elofsson, T. Sterner, and J. Åkerman, "International and national climate policies for aviation: a review," *Climate Policy*, vol. 19, no. 6, pp. 787–799, 2019. [Online]. Available: https://doi.org/10.1080/14693062.2018.1562871

[4] W. T. G. on Environmental Health Criteria for Noise and W. H. Organization, "Noise," p. Published under the joint sponsorship of the United Nations Environment Programme and the World Health Organization, 1980.

[5] E. Commission, *Flightpath 2050: Europe's Vision for Aviation—Report of the High-Level Group on Aviation Research*, EU Publications, Luxembourg, 2012. [Online]. Available: https://op.europa.eu/en/publication-detail/-/publication/7d834950-1f5e-480f-ab70-ab96e4a0a0ad/language-en

[6] NASA Aeronautics, "NASA Aeronautics Strategic Implementation Plan 2019 Update," National Aeronautics and Space Administration (NASA), Tech. Rep. NP-2017-01-2352-HQ, 2019.

[7] J. Rosero, J. Ortega, E. Aldabas, and L. Romeral, "Moving towards a more electric aircraft," *IEEE Aerospace and Electronic Systems Magazine*, vol. 22, no. 3, pp. 3–9, 2007.

[8] J. Weimer, "Electrical power technology for the more electric aircraft," in *[1993 Proceedings] AIAA/IEEE Digital Avionics Systems Conference*, 1993, pp. 445–450.

[9] J. Bailey, "The top 5 most produced commercial aircraft in history," Dec 2020. [Online]. Available: https://simpleflying.com/the-top-5-most-produced-commercial-aircraft-in-history/

[10] "Boeing next-generation 737," 2021. [Online]. Available: https://www.boeing.com/commercial/737ng/

[11] S. Trimble, "Boeing revises "obsolete" performance assumptions," Aug 2015. [Online]. Available: https://www.flightglobal.com/boeing-revises-obsolete-performance-assumptions/117817.article

[12] B. GRAVER, D. RUTHERFORD, and S. ZHENG, "Co2 emissions from commercial aviation for 2013, 2018 and 2029," Oct 2020. [Online]. Available: https://theicct.org/sites/default/files/publications/CO2-commercial-aviation-oct2020.pdf

[13] "Greenhouse gas emissions from a typical passenger vehicle," Mar 2018. [Online]. Available: https://www.epa.gov/greenvehicles/greenhouse-gas-emissions-typical-passenger-vehicle

[14] P. Wheeler and S. Bozhko, "The more electric aircraft: Technology and challenges." *IEEE Electrification Magazine*, vol. 2, no. 4, pp. 6–12, 2014.

[15] J. P. Sutherland, *Fly-by-wire flight control systems*. Defense Technical Information Center, 1968.

[16] S. F. Clark, "787 propulsion system." [Online]. Available: https://www.boeing.com/commercial/aeromagazine/articles/2012_q3/2/

[17] C. Adams, "A380: 'more electric' aircraft," Oct 2001. [Online]. Available: https://www.aviationtoday.com/2001/10/01/a380-more-electric-aircraft/

[18] B. J. Brelje and J. R. Martins, "Electric, hybrid, and turboelectric fixed-wing aircraft: A review of concepts, models, and design approaches," *Progress in Aerospace Sciences*, vol. 104, pp. 1–19, 2019. [Online]. Available: https://www.sciencedirect.com/science/article/pii/S0376042118300356

[19] M. A. Rendón, C. D. Sánchez R., J. Gallo M., and A. H. Anzai, "Aircraft hybrid-electric propulsion: Development trends, challenges and opportunities," *Journal of Control, Automation and Electrical Systems*, vol. 32, no. 5, pp. 1244–1268, Oct 2021. [Online]. Available: https://doi.org/10.1007/s40313-021-00740-x

[20] D. Finger, C. Braun, and C. Bil, "Comparative assessment of parallel-hybrid-electric propulsion systems for four different aircraft," in *Aircraft Design Under Consideration of Hybrid-Electric Propulsion Technology*, 01 2020.

[21] "(starc-abl) single-aisle turboelectric aircraft with aft boundary-layer propulsion." [Online]. Available: https://sacd.larc.nasa.gov/asab/asab-projects-2/starc-abl/

[22] H. Schefer, L. Fauth, T. H. Kopp, R. Mallwitz, J. Friebe, and M. Kurrat, "Discussion on electric power supply systems for all electric aircraft," *IEEE Access*, vol. 8, pp. 84 188–84 216, 2020.

[23] L. Gipson, "Hybrid wing body goes hybrid," Feb 2013. [Online]. Available: https://www.nasa.gov/content/hybrid-wing-body-goes-hybrid

[24] J. L. Felder, "Nasa n3-x with turboelectric distributed propulsion." [Online]. Available: https://ntrs.nasa.gov/api/citations/20150002081/downloads/20150002081.pdf

[25] F. F. da Silva, J. F. P. Fernandes, and P. J. da Costa Branco, "Barriers and challenges going from conventional to cryogenic superconducting propulsion for hybrid and all-electric aircrafts," *Energies*, vol. 14, no. 21, 2021. [Online]. Available: https://www.mdpi.com/1996-1073/14/21/6861

[26] X. Zhang, C. L. Bowman, T. C. O'Connell, and K. S. Haran, "Large electric machines for aircraft electric propulsion," *IET Electric Power Applications*, vol. 12, no. 6, pp. 767–779, 2018. [Online]. Available: https://ietresearch.onlinelibrary.wiley.com/doi/abs/10.1049/iet-epa.2017.0639

[27] K. O'Connor, "Pipistrel earns first electric aircraft type certificate," Jun 2020. [Online]. Available: https://www.avweb.com/aviation-news/pipistrel-earns-first-electric-aircraft-type-certificate/

[28] "Velis electro: Arriving from the future, easa type-certified now." [Online]. Available: https://www.pipistrel-aircraft.com/aircraft/electric-flight/velis-electro-easa-tc/

[29] Ángel Arcos-Vargas, D. Canca, and F. Núñez, "Chapter 12 - business opportunities in the day ahead markets by storage integration: An application to the german case," in *Mathematical Modelling of Contemporary Electricity Markets*, A. Dagoumas, Ed. Academic Press, 2021, pp. 209–224. [Online]. Available: https://www.sciencedirect.com/science/article/pii/B9780128218389000128

[30] S. HYMEL, "What is a battery?" [Online]. Available: https://learn.sparkfun.com/tutorials/what-is-a-battery/all

[31] "Bu-808c: Coulombic and energy efficiency with the battery," Nov 2021. [Online]. Available: https://batteryuniversity.com/article/bu-808c-coulombic-and-energy-efficiency-with-the-battery

[32] K. Provazi, B. A. Campos, D. C. R. Espinosa, and J. A. S. Tenório, "Metal separation from mixed types of batteries using selective precipitation and liquid–liquid extraction techniques," *Waste Management*, vol. 31, no. 1, pp. 59–64, 2011. [Online]. Available: https://www.sciencedirect.com/science/article/pii/S0956053X10004460

[33] J. Xu, H. Thomas, R. W. Francis, K. R. Lum, J. Wang, and B. Liang, "A review of processes and technologies for the recycling of lithium-ion secondary batteries," *Journal of Power Sources*, vol. 177, no. 2, pp. 512–527, 2008. [Online]. Available: https://www.sciencedirect.com/science/article/pii/S0378775307026195

[34] G. Dorella and M. B. Mansur, "A study of the separation of cobalt from spent li-ion battery residues," *Journal of Power Sources*, vol. 170, no. 1, pp. 210–215, 2007. [Online]. Available: https://www.sciencedirect.com/science/article/pii/S0378775307007446

[35] A. Mohamed, "Modeling, simulation and fault diagnosis in a microgrid," Ph.D. dissertation, Faculty of Engineering at Cairo University, January 2016.

[36] X. Hu, C. Zou, C. Zhang, and Y. Li, "Technological developments in batteries: A survey of principal roles, types, and management needs," *IEEE Power and Energy Magazine*, vol. 15, no. 5, pp. 20–31, 2017.

[37] P. Geantil, "Top 5 factors that affect industrial battery efficiency," Sep 2020. [Online]. Available: https://www.fluxpower.com/blog/top-5-factors-that-affect-industrial-battery-efficiency

[38] B. Qin, Z. Liu, G. Ding, Y. Duan, C. Zhang, and G. Cui, "A single-ion gel polymer electrolyte system for improving cycle performance of limn2o4 battery at elevated temperatures," *Electrochimica Acta*, vol. 141, pp. 167–172, 2014. [Online]. Available: https://www.sciencedirect.com/science/article/pii/S0013468614013802

[39] R. O'Hayre, S. Cha, W. Colella, and F. Prinz, *Fuel Cell Fundamentals*. Wiley, 2016. [Online]. Available: https://books.google.nl/books?id=O2JYCwAAQBAJ

[40] O. Z. Sharaf and M. F. Orhan, "An overview of fuel cell technology: Fundamentals and applications," *Renewable and Sustainable Energy Reviews*, vol. 32, pp. 810–853, 2014. [Online]. Available: https://www.sciencedirect.com/science/article/pii/S1364032114000227

[41] S. Mekhilef, R. Saidur, and A. Safari, "Comparative study of different fuel cell technologies," *Renewable and Sustainable Energy Reviews*, vol. 16, no. 1, pp. 981–989, 2012. [Online]. Available: https://www.sciencedirect.com/science/article/pii/S1364032111004709

[42] Y. Fan, H. Hu, and H. Liu, "Enhanced coulombic efficiency and power density of air-cathode microbial fuel cells with an improved cell configuration," *Journal of Power Sources*, vol. 171, no. 2, pp. 348–354, 2007. [Online]. Available: https://www.sciencedirect.com/science/article/pii/S0378775307013419

[43] W. Chen, Z. Liu, Y. Li, X. Xing, Q. Liao, and X. Zhu, "Improved electricity generation, coulombic efficiency and microbial community structure of microbial fuel cells using sodium citrate as an effective additive," *Journal of Power Sources*, vol. 482, p. 228947, 2021. [Online]. Available: https://www.sciencedirect.com/science/article/pii/S0378775320312465

[44] "Battery cell comparison." [Online]. Available: https://www.epectec.com/batteries/cell-comparison.html

[45] S. T. Revankar, “Chapter six - chemical energy storage,” in *Storage and Hybridization of Nuclear Energy*, H. Bindra and S. Revankar, Eds. Academic Press, 2019, pp. 177–227. [Online]. Available: https://www.sciencedirect.com/science/article/pii/B9780128139752000065

[46] B. G. Pollet, I. Staffell, and J. L. Shang, “Current status of hybrid, battery and fuel cell electric vehicles: From electrochemistry to market prospects,” *Electrochimica Acta*, vol. 84, pp. 235–249, 2012, eLECTROCHEMICAL SCIENCE AND TECHNOLOGYState of the Art and Future PerspectivesOn the occasion of the International Year of Chemistry (2011). [Online]. Available: https://www.sciencedirect.com/science/article/pii/S0013468612005671

[47] X. Jin, M. Guo, R. E. White, and K. Huang, “Understanding power enhancement of SOFC by built-in chemical iron bed: A computational approach,” *Journal of The Electrochemical Society*, vol. 164, no. 11, pp. E3054–E3062, 2017. [Online]. Available: https://doi.org/10.1149/2.0071711jes

[48] “What are brushless dc motors.” [Online]. Available: https://www.renesas.com/us/en/support/engineer-school/brushless-dc-motor-01-overview

[49] M. C. O. M. Team, “Brushed dc motors vs. brushless dc motors,” Jan 2017. [Online]. Available: https://www.automate.org/blogs/brushed-dc-motors-vs-brushless-dc-motors

[50] A. E. Fitzgerald, C. Kingsley, and S. D. Umans, *Electric Machinery*. McGraw-Hill, 2009.

[51] E. Staff, “Basics of ac induction motors,” Jul 2017. [Online]. Available: https://instrumentationtools.com/basics-ac-induction-motors/

[52] D. Levkin, “Permanent magnet synchronous motor.” [Online]. Available: https://en.engineering-solutions.ru/motorcontrol/pmsm/

[53] M. Lindegger, P. H.-P. Binera, B. Evéquoz, and P. D. D. Salathé, “Economic feasibility, applications and limits of efficient permanent-magnet motors,” Jul 2006.

[54] C. Detloff, “Ac induction motors vs. permanent magnet synchronous motors,” Jan 2017. [Online]. Available: https://empoweringpumps.com/ac-induction-motors-versus-permanent-magnet-synchronous-motors-fuji

[55] “Difference between induction motor and synchronous motor.” [Online]. Available: https://circuitglobe.com/difference-between-induction-motor-and-synchronous-motor.html

[56] P. K. Johnson, “Model aircraft propellers,” 2003. [Online]. Available: https://www.airfieldmodels.com/information_source/model_aircraft_engines/propellers.htm

[57] D. Lawhorn, V. Rallabandi, and D. M. Ionel, “Electric aircraft system co-simulation including body, propeller, propulsion, and energy storage models,” in *2019 IEEE Transportation Electrification Conference and Expo (ITEC)*, 2019, pp. 1–5.

[58] E. M. Greitzer, Z. S. Spakovszky, and I. A. Waitz, “11.7 performance of propellers.” [Online]. Available: https://web.mit.edu/16.unified/www/FALL/thermodynamics/notes/node86.html

[59] E. Konuk, “Trajectory Simulation With Battery Modeling for Electric Powered Unmanned Aerial Vehicles,” Master’s thesis, OLD DOMINION UNIVERSITY, May 2020.

[60] “Performance data,” Mar 2021. [Online]. Available: https://www.apcprop.com/technical-information/performance-data/

[61] D. G. Hull, *Fundamentals of Airplane Flight Mechanics*, 1st ed. Springer Publishing Company, Incorporated, 2007.

[62] C. Huynh, L. Zheng, and D. Acharya, “Losses in High Speed Permanent Magnet Machines Used in Microturbine Applications,” *Journal of Engineering for Gas Turbines and Power*, vol. 131, no. 2, 12 2008, 022301. [Online]. Available: https://doi.org/10.1115/1.2982151

[63] T. Hobbies. [Online]. Available: https://www.towerhobbies.com/product/avistar-elite-.46-55-gpep-62.5-arf/GPMA1005.html

[64] “Rimfire .46 42-60-800 outrunner brushless.” [Online]. Available: https://www.towerhobbies.com/product/rimfire-.46-42-60-800-outrunner-brushless/GPMG4725.html#

[65] “Team corally sport racing 50c 5400mah 4s 14,8v lipo battery.” [Online]. Available: https://www.eurorc.com/product/28451

[66] Z. M. Salameh and B. G. Kim, “Advanced lithium polymer batteries,” in *2009 IEEE Power & Energy Society General Meeting*, 2009, pp. 1–5.

[67] L. Butcher, “Pipistrel alpha electro - e-mobility engineering,” Oct 2021. [Online]. Available: https://www.emobility-engineering.com/pipistrel-alpha-electro/

[68] J. Scott, “Ask us - drag coefficient & lifting line theory.” [Online]. Available: http://www.aerospaceweb.org/question/aerodynamics/q0184.shtml

[69] “Aircraft information - pipistrel alpha electro,” Oct 2017. [Online]. Available: www.pipistrel-usa.com/wp-content/uploads/2018/03/Pipistrel-Alpha-ELECTRO-Information-Pack.pdf

[70] “Easa.a.573 - virus sw 121.” [Online]. Available: https://www.easa.europa.eu/document-library/type-certificates/aircraft-cs-25-cs-22-cs-23-cs-vla-cs-lsa/easaa573-virus-sw-121

[71] O. Bergmann, F. Götten, C. Braun, and F. Janser, "Comparison and evaluation of blade element methods against rans simulations and test data," *CEAS Aeronautical Journal*, vol. 13, no. 2, pp. 535–557, Apr 2022. [Online]. Available: https://doi.org/10.1007/s13272-022-00579-1

[72] "Pipistrel p-812-164-f3a propeller." [Online]. Available: https://www.pipistrel-aircraft.com/aircraft/other-products/propellers/

[73] "Emrax electric motors / generators." [Online]. Available: https://emrax.com/e-motors/

[74] "E-811 electrical engine." [Online]. Available: https://www.pipistrel-aircraft.com/aircraft/electric-flight/e-811/#tab-id-2

[75] "Batteries systems and bms." [Online]. Available: https://www.pipistrel-aircraft.com/aircraft/electric-flight/batteries-systems-and-bms/

[76] L. Somer, "Lsrpm - plsrpm - kmc.co.rs." [Online]. Available: http://kmc.co.rs/sites/default/files/DYNEO_LSRPM_4122f_en_2011.02_0.PDF

[77] A. ACW, "Bombardier (de havilland) dash 8 q-400," Jan 2013. [Online]. Available: https://avioesemusicas.com/bombardier-de-havilland-dash-8-q-400.html

[78] Y. Zhang, H. Chen, and Y. Zhang, "Wing optimization of propeller aircraft based on actuator disc method," *Chinese Journal of Aeronautics*, vol. 34, 01 2021.

[79] "Bombardier dash 8 q400." [Online]. Available: https://www.airlines-inform.com/commercial-aircraft/dash-8q400.html

[80] "Bombardier q400 propeller - dowty r408," Sep 2011. [Online]. Available: https://www.flyradius.com/bombardier-q400/propeller-dowty-r408

[81] Z. Liu, P. Liu, Q. Qu, and T. Hu, "Effect of advance ratio and blade planform on the propeller performance of a high altitude airship," *Journal of Applied Fluid Mechanics*, vol. 9, no. 6, pp. 2993–3000, 2016. [Online]. Available: https://www.jafmonline.net/article_1862.html

[82] P. Roshanfekr, T. Thiringer, M. Alatalo, and S. Lundmark, "Performance of two 5 mw permanent magnet wind turbine generators using surface mounted and interior mounted magnets," in *2012 XXth International Conference on Electrical Machines*, 2012, pp. 1041–1047.

[83] M. Filipenko, L. Kühn, T. Gleixner, M. Thummet, M. Lessmann, D. Möller, M. Böhm, A. Schröter, K. Häse, J. Grundmann, M. Wilke, M. Frank, P. van Hasselt, J. Richter, M. Herranz-Garcia, C. Weidermann, A. Spangolo, M. Klöpzig, P. Gröppel, and S. Moldenhauer, "Concept design of a high power superconducting generator for future hybrid-electric aircraft,"

Superconductor Science and Technology, vol. 33, no. 5, p. 054002, mar 2020. [Online]. Available: https://doi.org/10.1088/1361-6668/ab695a

[84] Y. Zhang, Y. Cheng, R. Qu, D. Li, Y. Gao, and Q. Wang, “Ac loss analysis and modular cryostat design of a 10-mw high-temperature superconducting double stator flux modulation machine,” *IEEE Transactions on Industry Applications*, pp. 1–9, 2022.